Omicron BA.5 infects human brain organoids and is neuroinvasive and lethal in K18-hACE2 mice

Romal Stewart[1#], Sevannah A. Ellis[2,#], Kexin Yan[1,#], Troy Dumenil[1,#], Bing Tang[1], Wilson Nguyen[1], Cameron Bishop[1], Thibaut Larcher[3], Rhys Parry[4], Robert K. P. Sullivan[2], Mary Lor[1], Alexander A. Khromykh[4,5], Frédéric A. Meunier[2,5,†], Daniel J. Rawle[1,†], Andreas Suhrbier[1,5,†].

[1] QIMR Berghofer Medical Research Institute, Brisbane, Queensland. 4029, Australia.

[2] Clem Jones Centre for Ageing Dementia Research, Queensland Brain Institute, The University of Queensland, Brisbane, Queensland, Australia.

[3] INRAE, Oniris, PAnTher, APEX, Nantes, France.

[4] School of Chemistry and Molecular Biosciences, University of Queensland Brisbane QLD Australia.

[5] Australian Infectious Disease Research Centre, GVN Center of Excellence, Brisbane, Queensland 4029 and 4072, Australia.

[#] Joint first authors

[†] Joint last authors

[*]Co-corresponding authors. Email: Andreas. Suhrbier@qimrberghofer.edu.au and Frédéric A. Meunier

Keywords:

SARS-CoV-2, omicron, BA.5, K18-hACE2, brain

ABSTRACT

A frequently repeated premise is that viruses evolve to become less pathogenic. This appears also to be true for SARS-CoV-2, although the increased level of immunity in human populations makes it difficult to distinguish between reduced intrinsic pathogenicity and increasing protective immunity. The reduced pathogenicity of the omicron BA.1 sub-lineage compared to earlier variants is well described and appears to be due to reduced utilization of TMPRRS2. That this reduced pathogenicity remains true for omicron BA.5 was recently reported. In sharp contrast, we show that a BA.5 isolate was significantly more pathogenic in K18-hACE2 mice than a BA.1 isolate, with BA.5 infection showing increased neurovirulence, encephalitis and mortality, similar to that seen for an original ancestral isolate. BA.5 also infected human cortical brain organoids to a greater extent than a BA.1 and original ancestral isolate. Neurons were the target of infection, with increasing evidence of neuron infection in COVID-19 patients. These results argue that while omicron virus may be associated with reduced respiratory symptoms, BA.5 shows increased neurovirulence compared to earlier omicron sub-variants.

Introduction

The omicron variant of concern diverges considerably from earlier variants; the evolutionary origins remain unclear, with the closest genetic ancestor dating back to mid-2020 [1,2]. Omicron viruses have spread faster globally than any previous variants, and the BA.5 sub-lineage became the dominant SARS-CoV-2 virus in many countries [3,4]. Long COVID is now well described for many variants of concern [5], and also occurs after infection with BA.5 [6]. Neurological and psychiatric manifestations represent a major component of COVID-19 and long COVID [7-9] and these remain for patients infected with omicron viruses [10-13], although data specifically for BA.5 neurological manifestations has not yet emerged. The large number of changes in spike for omicron and omicron sub-lineages has rendered vaccination [14-16], many monoclonal antibody treatments [17], and prior exposure with other variants [18] less protective. Patients who experience multiple SARS-CoV-2 infections are also at increased risk of acute and post-acute sequalae, which include neurological manifestations [19].

There is strong evidence for brain abnormalities in COVID-19 patients [20-23]. Encephalitis is well documented, usually in hospitalized COVID-19 patients with severe disease, with encephalitis predisposing to poor outcomes and a higher risk of mortality [9,24-26]. The mechanism(s) whereby brain pathology/immunopathology and/or neuropathology might manifest in COVID-19 patients remains debatable, with the systemic cytokine storm and/or direct brain infection likely involved [22,27-32]. A number of studies have now shown brain infection in COVID-19 patients [33-37], with viral RNA or protein detected in the brains of 20-38% of patients that died of COVID-19 [38,39]. A number of groups have also reported detection of viral RNA in cerebrospinal fluid of COVID-19 patients [40-44], including patients infected with omicron virus [45].

The K18-hACE2 mouse model represents a model of severe COVID-19 that significantly recapitulates the lung pathology and inflammatory pathways seen in humans, and has been widely used for assessing new interventions and for studying SARS-CoV-2 biology [46-48]. Infection of K18-hACE2 mice with original ancestral isolates via intranasal inoculation, usually results in fulminant and lethal brain infections, with virus likely entering the brain via the olfactory epithelium, across the cribriform plate and into the olfactory bulb [49-54]. This route of entry into the brain may also be relevant for COVID-19 patients [35,38,39,55-57].

Neurons represent a target of SARS-CoV-2 infection in brains of K18-hACE2 mice [50,58], non-human primates [57], and hamsters [59], with infection of neurons also observed in COVID-19

patients [34,36,37]. Reduced brain infection and the ensuing reduction in mortality after infection of K18-hACE2 mice with omicron BA.1 [60-62] or BA.5 viruses [63,64] has been viewed as evidence that these viruses are intrinsically less pathogenic [65,66]. Similarly, a chimeric original ancestral virus containing a BA.1 spike showed 80% lethality in K18-hACE2 mice, whereas BA.1 infection was non-lethal, arguing that non-spike proteins can carry determinants of pathogenicity [67]. The latter contention is supported by other studies that do not involve mice [68,69]. Establishing lower pathogenicity of new variants in humans populations is complicated by the rising levels of protective immunity due to vaccinations and/or past infections [66,70]. *In vitro* organoid systems provide another method for evaluating pathogenicity, with infection of neurons in brain organoids well described [37,71,72], and BA.2 showing enhanced replication [73]. Infection of neurons results in their demise [71,72], with type I IFN induction seen in some studies [72,73] but not others [37].

Evasion of anti-spike antibodies is likely the main driver of SARS-CoV-2 evolution, as the majority of amino acid substitutions in new variants are in the spike protein [74,75]. However, changes in non-spike proteins are likely responsible for the increasing resistance to the anti-viral activity of type I interferons seen for each new variant of concern [68], with a sizable number of SARS-CoV-2 non-spike proteins involved in suppressing these responses [69,76].

Herein we show that an omicron BA.1 isolate was significantly less pathogenic in K18-hACE2 than an original ancestral isolate, in agreement with previous reports [60-62]. A recent publication reports that this reduced pathogenicity remains true for omicron BA.5 [63]. In contrast, when compared with BA.1, we found that a BA.5 isolate displayed increased pathogenicity in K18-hACE2 mice, with rapid weight loss, brain infection and encephalitis, and mortality. In addition, BA.5 productively infected human brain organoids significantly better than BA.1. These results suggest that the omicron lineage is not evolving towards reduced pathogenicity, with BA.5 showing increased neuropathology over BA.1.

Results

Omicron BA.5 is lethal in K18-hACE2 mice

Infection of K18-hACE2 mice with original ancestral isolates of SARS-CoV-2 is well described and results in weight loss and mortality by ≈5 days post infection (dpi) [52,53,77-80]. We re-illustrate this phenomena herein using an original ancestral isolate (SARS-CoV-2_{QLD02}) and

our K18-hACE2 mice, with the ethically defined end point of >20% weight loss reached by 4-5 days post infection (dpi) (Fig. 1a, Original). An omicron BA.1 isolate (SARS-CoV-2_{QIMR01}) was substantially less virulent, with only 20% of mice showing weight loss >20% requiring euthanasia by 9/10 dpi (Fig. 1a, Omicron BA.1; Supplementary Fig. 1a). The reduced pathogenicity of BA.1 isolates in K18-hACE2 mice is consistent with previous reports [60-62,67].

Infection of K18-hACE2 mice with an omicron BA.5 virus (SARS-CoV-2_{QIMR03}) resulted in severe weight loss requiring euthanasia in 100% of mice by 4-6 dpi (Fig. 1a, Omicron BA.5). BA.5 infected mice also showing more overt symptoms than BA.1, with original ancestral isolate showing slightly higher disease scores than BA.5 (Fig. 1b). Kaplan Meier plots illustrate a highly significant difference between BA.5 and BA.1 (Fig. 1b, $p=1.7x10^{-9}$). Although mortality from BA.5 was significantly delayed when compared with the original ancestral isolate ($p=0.003$), the mean delay was only 0.88 days (Fig. 1c). These results contrast with a recent publication reporting that the reduced pathogenicity of omicron sub lineages was retained for BA.5 [63].

On 5 dpi there were no significant differences in viral titers in lungs and nasal turbinates between BA.1 and BA.5, whereas the original ancestral isolate had ≈2 logs higher lung titers and ≈4 logs higher nasal turbinate titers (Fig. 1d, $p\leq0.034$ Kruskal-Wallis tests). Brain titers were also ≈4 logs higher on 5 dpi for the original ancestral isolate when compared with BA.5, with BA.5 titers not significantly different from the BA.1 brain titers for the 3 mice that were euthanized due to weight loss 9/10 dpi (Fig. 1d, Brains). However, consistent with previous reports [58,81], the majority (80%) of BA.1 infected mice showed no symptoms, with no virus detected in the brains of symptom-free animals (Fig. 1d, Brains).

Immunohistochemistry of BA.5 brain infection in K18-hACE2 mice

The fulminant brain infection seen after infection of K18-hACE2 mice with original ancestral isolates is well described, with widespread infection of neurons in various brain regions, including the cortex [49,50,52,54,58]. A very similar pattern of brain infection was observed in our hands using our K18-hACE2 mice and original ancestral isolate, with immunohistochemistry (IHC) undertaken using a recently developed anti-spike monoclonal antibody [54] (Supplementary Fig. 2a).

IHC staining of brains of K18-hACE2 mice infected with BA.5 also showed widespread

infection of neurons in the cortex, as well as the hippocampus and the hypothalamus (Fig. 2a,b). Viral RNA/protein has been detected in the cortex of post-mortem COVID-patients [36,37], with disruption of the hippocampus also reported [22,82]. The hypothalamus does not appear to be the site of infection in COVID-19 patients [83], although the hypothalamic-pituitary axis does appear to be affected [84]. Viral antigen was also clearly evident in neural dendrites and axons (Fig. 2b), with viral antigen staining in neurites previously shown in human brain organoids [85].

In the K18-hACE2 model, brain infection is generally associated with weight loss and mortality [86] (generally via euthanasia after reaching ethically defined end points). Perhaps of note, even low levels of IHC-detectable BA.5 infection was associated with weight loss that required euthanasia (Supplementary Fig. 2b), illustrating that such fatal outcomes do not require a fulminant brain infection.

Lesions in the brains of BA.5 infected K18-hACE2 mice identified by H&E staining

The brains of BA.5 infected K18-hACE2 mice showed a number lesions that have also been observed in COVID-19 patients and/or primate models. Neuron vacuolation (hydropic degeneration) was clearly evident (Fig. 3a), and has been reported previously for infection of K18-hACE2 mice with an original ancestral isolate [49], and was also observed in non-human primate (NHP) model of SARS-CoV-2 infection [31]. The presence of viral antigen in the cortex was associated with apoptosis (Supplementary Fig. 3) and a high intensity of H&E-detectable lesions (primarily vacuolation), but was not associated with immune cell infiltrates (Supplementary Fig. 4). The lack of infiltrates around areas of infection has also been noted in COVID-19 patients [37]. Perivascular cuffing (Fig. 3b) is well described in histological examinations of brains from deceased COVID-19 patients [38,39,56,87,88]. Other lesions observed in the BA.5-infected K18-hACE2 mouse brains, that have also been described in post-mortem COVID-19 patients, include perivascular edema (Fig. 3c) [89-91], microglial nodules (Fig. 3d) [38,56,88,92], and small hemorrhagic lesions (Fig. 3e) [87,93].

SARS-CoV-2 Omicron BA.5 infects neurons in K18-hACE2 mice

Infection in the brains of K18.hACE2 mice with BA.5 is primarily located within the cortex as revealed using S-protein immunocytochemistry (Fig. 4 a-f). We used co-staining with the neuronal marker NeuN and SARS-CoV-2 S-protein which was mainly detected in neurons

demonstrating that they are the primary target cells in K18-hACE2 mouse brains (Fig 4. a-f). These neurons were predominantly found in layer 6 and are therefore likely pyramidal neurons. Using super-resolution microscopy, we resolved S-protein within vesicular structures in the neuronal cell bodies (Fig. 4 d-f insets). We also found low levels of S-protein in microglia labelled with Iba1 (Fig. 4 g-l). This suggests that microglia may also be infected, albeit at low levels, or that actively phagocytose viral particles (Fig. 4 j-l insets). Furthermore, microglia appear to be recruited to infected neurons and their processes making immediate contact with infected cells (Fig. 4 j-l insets). Interestingly, we could not detect signs of infection of reactive astrocytes labelled with GFAP in immediate proximity to infected neurons (Fig 4 m-r and insets).

RNA-Seq of BA.5-infected K18-hACE2 mouse brains

Mice were infected i.n. as in Fig. 1 (BA.5) and euthanized when weight loss reached the ethically defined end point of ≈20% (Supplementary Fig. 5a). Control mice received the same i.n. inoculation of UV-inactivated BA.5. Brains were examined by RNA-Seq (BioProject ID: PRJNA911424), with the PCA plot shown in Supplementary Fig. 5b and viral reads in Supplementary Fig. 5c. Differentially expressed genes (DEGs) ($q<0.05$, n=437) were analyzed by Ingenuity Pathway Analysis (IPA) [46,53] (Supplementary Table 1). Selected representative IPA annotations, grouped by themes, are shown in Fig. 5. The dominant annotations illustrate a cytokine storm, with the top cytokine Up Stream Regulators (USRs) including interferons both type II (IFNγ) and type I (IFNα2, IFNλ1 IFNβ1), as well as TNF, IL-1 and IL-6, all previously well described for SARS-CoV-2 infections [46]. The concordance for cytokine USRs for brain and lung infection and for the different variants of concern was high (Supplementary Fig. 5d), arguing that inflammatory response are generally very similar across different infected organs and for different SARS-CoV-2 variants.

A large series of annotations were associated with leukocyte migration and activation (Supplementary Table 1), with the top two overarching annotations shown (Fig. 5). These results are consistent with the perivascular cuffing seen by H&E (Fig. 3b). An additional series of neuropathology-associated annotations were also identified with high z-scores and significance (Fig. 5, Neuropathology). Activation of microglia and vascular lesions (Fig. 5) were consistent with the histological findings (Fig. 3b,c,d). Multiple sclerosis-like features, myelitis, demyelination [94,95] and encephalitis [9,24-26] are also features described for COVID-19 patients.

Apoptosis of neurons was reported in the NHP model [31], with pyroptosis in the CNS of COVID-19 patients also proposed [96]. Gene Set Enrichment Analyses (GSEAs) using gene sets provided in MSigDB (≈50,000 gene sets) and in Blood Transcription Modules [97], generated broadly comparable results to those obtained from IPA (Supplementary Table 1). In addition, a significant negative enrichment (negative NES) for olfactory neuroepithelium genes (MSigDB) [98] was also identified (Fig. 5), suggesting loss of cells in this tissue in BA.5-infected mouse brains.

In summary, the bioinformatic analyses suggest that BA.5-infected K18-hACE2 mouse brains show typical SARS-CoV-2-associated inflammatory responses, with annotations consistent with histological findings and studies in COVID-19 patients.

Human cortical brain organoids

Human, induced pluripotent cells (hiPSCs), derived from a primary dermal fibroblast line (HDFa) from a normal human adult, were used to generate approximately spherical, ≈2-3 mm diameter, "mini-brains" using a rotating incubator (Supplementary Fig. 6a). Thirty day old organoids were infected with either the original ancestral isolate, BA.1 or BA.5 (MOI≈1) and were cultured for 4 days. IHC illustrated that substantially more cells in the organoids were infected by BA.5 than by the original ancestral virus (Fig. 6a). The small area infected with the original ancestral isolate (Fig. 6a, Original, insert) corresponded to an area of the organoid with IHC-detectable hACE2 staining (Supplementary Fig. 6b). Supernatants showed a significant increase in viral titers after BA.5 infection over the 4 day period, and virus titer in the supernatant was significantly higher for BA.5 compared to BA.1 at day 4 post infection (Fig. 6b). RNA-Seq was undertaken on organoids 4 dpi and viral reads were ≈25 fold higher for organoids infected with BA.5 than those infected with an original ancestral isolate (Fig. 6c).

RNA-Seq of BA.5 infected human cortical brain organoids compared with uninfected organoids provided 2390 DEGs ($q<0.001$), of which 575 were up-regulated genes (Supplementary Table 2). RNA-Seq of original ancestral isolate-infected organoids provided 252 DEGs ($q<0.001$), of which 132 were up-regulated (Supplementary Table 2). Given the higher level of infection, more DEGs might be expected for BA.5. Of the 132 up-regulated DEGs, 118 were also identified in the BA.5 infected organoids (Fig. 6d), arguing that the original ancestral is not inducing fundamentally different response in these organoids.

The 2390 DEGs for BA.5 were analyzed by IPA (Supplementary Table 2), with "Coronavirus Pathogenesis Pathway" identified as a top canonical pathway (Fig. 6e). The top USRs were (i) PTPRR (a protein tyrosine phosphatase receptor), which was recently identified in a study of brains from SARS-CoV-2 infected hamsters and is associated with depression in humans [99], (ii) COPS5 (COP9 signalosome subunit 5), whose mRNA is bound by SARS-CoV-2 NSP9, perhaps resulting in suppression of host responses [100], (iii) LARP1, a translational repressor that binds SARS-CoV-2 RNA [101], (iv) ESR1 (nuclear estrogen receptor), which is important for ACE2 expression [102], (v) EGLIN, oxygen sensors that target HIF α subunits for degradation, with HIF-1α promoting SARS-CoV-2 infection and inflammation [103]. IPA Diseases and Functions feature identified a series of neuropathology-associated annotations, including a motor dysfunction signature, with motor deficits documented for severe COVID-19 patients [21]. Consistent with the IHC data, a series of signatures describe disruption and death of neurons (Fig. 6e). No significant up-regulation of IFN, cytokine or inflammatory signatures was identified after infection with BA.5.

Discussion

We show herein that a BA.5 isolate is more pathogenic in K18-hACE2 mice than a BA.1 isolate, arguing that the reduced pathogenicity of omicron variants may not be retained by BA.5. Our observation contrasts with a previous report [63], but is consistent with recent hamster studies [104,105]. The COR-22 isolate used in the Uraki et al. study has two substitutions from the original ancestral not seen in the QIMR03 isolate used herein (Spike T76I, NSP5 P252L). The QIMR03 isolate (BE.1 sublineage) also has seven substitutions from the original ancestral not seen in COR-22; NS3 (Orf3a) G49C and V48F, NSP3 A386T, NSP2 Q376K and I273V, NSP13 M233I, N E136D. To the best of our knowledge no pertinent activities have been ascribed to these substitutions, although N, NSP3 and NSP13 are involved in suppression of type I IFN responses [76], which may provide an explanation for differences between COR-22 and QIMR03.

An increase in pathogenicity of BA.5 over BA.1 in K18-hACE2 mice may be associated with an increased reliance on TMPRSS2 [106]. The early omicron variants tended to be less dependent on TMPRSS2 than original ancestral isolates, and showed an increased propensity to use the endocytic route of entry; a shift associated with lower pathogenicity and changes in spike [107,108]. The BA.1 and BA.5 isolates used herein have 14 amino acid differences in the spike

protein (Supplementary Table 3). Pathogenicity has been shown to be dependent on TMPRSS2 utilization [109], with TMPRSS2 utilization reported to be a virulence determinant, even for omicron variants [110]. Treatment with a TMPRSS2 inhibitor also prevented brain infection in K18-hACE2 mice [111]. An increased ability to infect, even TMPRSS2-low, cells in the olfactory epithelium [112] may thus promote entry of BA.5 into the brains of K18-hACE2 mice. What remains perplexing is how the TMPRSS2-dependent original ancestral isolate can produce such a fulminant brain infection, despite the low level expression (mean of only 3.6 reads) of TMPRSS2 (Supplementary Table 1, All genes tab, yellow highlight). Viral reads in K18-hACE2 mice infected with the original ancestral isolate illustrate a loss of the QTQTN sequence adjacent to the furin cleavage site, which impairs furin cleavage [113-115], in virus populations in the brain in half of the animals, but not the lung (Supplementary Fig. 7a). A furin cleavage site deletion is seen in virus sequences in brains of SARS-CoV-2 infected hamsters [116] (Supplementary Fig. 7b). Thus during brain infection the original ancestral isolate acquires a reduced dependence on TMPRSS2 [117]. BA.5 would thus appear to have both TMPRSS2-dependent and TMPRSS2-independent capabilities, the first perhaps promoting neurotropism and the second neurovirulence.

RNA-Seq of organoids illustrated zero or very low TMPRSS2 mRNA expression (PRJNA813692), explaining the very poor infection by the original ancestral isolate (Fig. 6a-c). The more efficient infection by BA.5 (Fig. 6a-c) was thus likely due to TMPRSS2-independent infection. Perhaps surprising was the lack of induction of type I IFN response by BA.5 in these organoids. However, a study using an original ancestral isolate also showed no IFN induction [37], whereas as an early, and a BA.2, omicron isolate induced clear type I IFN responses in slightly different organoid systems [72,73]. Our organoids are capable of generating type I IFN responses when infected with other viruses (Rawle *et al* in preparation), suggesting BA.5 can effectively suppress anti-viral response in this glia-free, neural organoid system. Suppression of type I IFN responses by SARS-CoV-2 involves multiple non-structural proteins [76], with a trend towards better suppression capabilities emerging with each new variant [68].

A widely repeated contention is that viruses tend to evolve towards lower virulence [118,119], even though there are good examples where this is clearly not the case [120-122]. For certain aspects the contention also does not appear to hold for SARS-CoV-2; for example, a higher proportion of patients infected with BA.5 develop anosmia, when compared with BA.1 [14]. Anosmia was

recently closely linked to long-lasting cognitive problems in COVID-19 patients [123], with infection of the olfactory epithelium potentially proving access to the brain [53,112]. The data herein would support the view that BA.5 has developed an increased propensity for neuroinvasiveness over earlier omicron variants. The detection of spike in infected brain cortical structures demonstrate that the SARS-CoV-2 can not only access these regions via an unknown mechanism but also selectively affect groups of neurons within these regions. It is worth noting that the detection of the S-protein in vesicular structures in the soma of pyramidal neurons suggest a possible transport mechanism that likely involve endocytosis and is potentially influenced by co-receptor neuropilin [124]. Further work is warranted to better understand this neuroinvasive mechanism as this likely contribute to neurological symptoms of COVID. Thus, even if respiratory disease is less severe for omicron variants as a whole, BA.5 may show increased risk of acute and long term neurological complications over earlier omicron variants [125].

Materials and methods

Ethics statements and regulatory compliance

All mouse work was conducted in accordance with the Australian code for the care and use of animals for scientific purposes (National Health and Medical Research Council, Australia). Mouse work was approved by the QIMR Berghofer Medical Research Institute Animal Ethics Committee (P3600). All infectious SARS-CoV-2 work was conducted in the BioSafety Level 3 (PC3) facility at the QIMR Berghofer MRI (Australian Department of Agriculture, Water and the Environment certification Q2326 and Office of the Gene Technology Regulator certification 3445). Breeding and use of GM mice was approved under a Notifiable Low Risk Dealing (NLRD) Identifier: NLRD_Suhrbier_Oct2020: NLRD 1.1(a). Mice were euthanized using carbon dioxide.

Collection of nasal swabs from consented COVID-19 patients was approved by the QIMR Berghofer Medical Research Institute Human Research Ethics Committee (P3600).

SARS-CoV-2 isolates

An original (ancestral) strain isolate, SARS-CoV-2_{QLD02} (hCoV-19/Australia/QLD02/2020)

(GISAID accession EPI_ISL_407896) was kindly provided by Dr Alyssa Pyke and Fredrick Moore (Queensland Health Forensic & Scientific Services, Queensland Department of Health, Brisbane, Australia) [126]. Omicron isolates were obtained from nasal swabs from consented COVID-19 patients [54,127]. Infected Vero E6 cells were subjected to RNA-Seq and viral genomes *de novo* assembled using Trinity. The omicron BA.1 isolate, SARS-CoV-2_{QIMR01} (SARS-CoV-2/human/AUS/QIMR03/2022), belongs to the BA.1.17 lineage (GenBank: ON819429 and GISAID EPI_ISL_13414183) [54,127]. The omicron BA.5 isolate, SARS-CoV-2_{QIMR03} (SARS-CoV-2/human/AUS/QIMR03/2022) belongs to the BE.1 sublineage (GenBank: OP604184.1). Virus stocks were propagated in Vero E6 cells and were checked for endotoxin and mycoplasma (MycoAlert, Lonza). Viruses were titered using $CCID_{50}$ assays [128].

Mouse infection and monitoring

K18-hACE2 mice (strain B6.Cg-Tg(K18-ACE2)2Prlmn/J, JAX Stock No: 034860) were purchased from The Jackson Laboratory, USA, and were maintained in-house as heterozygotes by backcrossing to C57BL/6J mice (Animal Resources Center, Canning Vale WA, Australia) as described [46]. Heterozygotes were inter-crossed to generate a homozygous K18-hACE2 transgenic mouse line. Genotyping was undertaken by PCR and sequencing across a SNP that associates with the hACE2 transgene [129] to distinguish heterozygotes (TTTG(A/C)AAAC) from homozygotes (TTTGCAAAC). The mice were held under standard animal house conditions, and were infected intrapulmonary via the nasal route with 5×10^4 $CCID_{50}$ of virus in 50 µL RPMI while under light anesthesia as described [53]. Mice were weighed and overt disease symptoms scored as described [53]. Mice were euthanized using CO_2, and tissue titers determined using $CCID_{50}$ assays and Vero E6 cells as described [53,126].

Maintenance and expansion of human induced pluripotent stem cells

The human-induced pluripotent cells (hiPSCs) used in this study were reprogrammed from adult dermal fibroblasts (HDFa, Gibco, C0135C) using the CytoTune-iPS 2.0 Sendai Reprogramming Kit (Invitrogen, A16518) [130]. They were cultured on human recombinant vitronectin (Thermo Fisher Scientific) coated plates in StemFlex medium (Thermo Fisher Scientific) according to the manufacturer's guidelines within a humidified tissue culture incubator at 37C, 5% CO_2 atmosphere.

Generation of Human Cortical organoids

On day 0 of organoid culture, hiPSCs (less than passage 50) were dissociated with StemPro Accutase (Thermo Fisher Scientific) to generate a cell suspension. 5000 cells were plated in each well of an ultra-low-binding 96-well plate (Corning) in StemFlex media supplemented with 10 µM ROCK inhibitor Y-27632 (Stemcell technologies). From days 1-5, daily media changes were carried out with StemFlex medium supplemented with 2 µM Dorsomorphine (Abcam) and 10 µM SB-431542 (Stemcell technologies). On day 5, the medium was replaced with a Neuroinduction medium consisting of DMEM/F12 (Thermo Fisher Scientific), 1% N2 Supplement (Thermo Fisher Scientific), 10 µg/ml Heparin (Stem cell technologies), 1% Penicillin/Streptomycin (Thermo Fisher Scientific), 1% Non-essential Amino Acids (Thermo Fisher Scientific), 1% Glutamax (Thermo Fisher Scientific) and 10 ng/ml FGF2 (Stemcell Technologies). On day 7, organoids were embedded in Matrigel (Corning), transferred to an ultra-low-binding 24-well plate (Corning) (one organoid per well), and continued to grow in Neuroinduction medium for three more days. On day 10, organoids were supplemented with differentiation medium, consisting of Neurobasal medium, 1% N2, 2% B27 supplements (Thermo Fisher Scientific), 0.5% Penicillin/Streptomycin, 1% Glutamax, 1% Non-essential Amino Acids, 50 µM of 2-Mercaptoenthanol (Merck), 2.5 µg/ml Insulin (Merck), 1% Knockout Serum Replacement (Thermo Fisher Scientific), 10ng/ml FGF2, 1 µM CHIR99021 (Stemcell Technologies) and placed in a CelVivo Clinostar incubator (Invitro Technologies) (24 organoids per Clinoreactor) spinning at 20 rpm. All media changes from 10 days onwards were performed every other day.

Infection of Cortical organoids

30-day-old organoids were transferred from each Clinoreactor into an ultra-low-binding 24-well plate (one organoid per well), infected with various SARS-CoV-2 strains at a multiplicity of infection (MOI) of 1 and placed within a humidified tissue culture incubator at 37C, 5% CO_2 for 2 hours. Organoids were then washed twice with media, transferred into 50 mm LUMOX gas exchange dishes (SARSTEDT) (4 organoids per dish) containing 7 ml of differentiation media, and placed within a humidified tissue culture incubator at 37C, 5% CO2 for 4 days.

Histology and immunohistochemistry

H&E staining of formalin fixed paraffin wax embedded tissue sections was undertaken as described [80,126]. Immunohistochemistry was undertaken as described using the in-house developed anti-spike monoclonal antibody, SCV-1E8 [54].

Fluorescence Immunohistochemistry

Paraffin embedded K18-hACE2 mouse brains were sectioned on a rotary microtome into 10 μm sagittal sections. Sections were dewaxed and antigen retrieval was performed in Antigen Recovery Solution (citrate buffer solution consisting of 10 mM Sodium Citrate, 0.05% SDS 0.01%, pH 6.0) at 90°C for 10 min in a BioCare decloaker. Slides were blocked with blocking buffer (0.5% BSA, 0.05% Saponin, 0.01% Triton X-100, 0.05% Sodium Azide in 0.1M Phosphate Buffered Saline (PBS) for 30 min at room temperature and subsequently incubated in primary antibody diluted in blocking buffer at room temperature for three days in a humidity chamber using anti-S-protein (mouse, 1:100, in house antibody SCV-1E8 [54]) in conjunction with either anti-NeuN (chicken, 1:3000, Merck, ABN91), anti-Iba1 (rabbit, 1:1000, Wako, #019-19741), or anti-GFAP (rabbit, 1:1000, Abcam, ab7260). Slides were washed 4 times in PBS for 15 min. Slides were further incubated in blocking buffer for 5 min prior to adding the species-specific secondary antibody at room temperature overnight in a light-proof humidity chamber: Alexa fluor-546 anti-mouse (1:1000, Invitrogen, A11030), Alexa fluor-647 anti-rabbit (1:1000, Invitrogen, A32733), or Alexa fluor-488 anti-chicken (1:1000, Invitrogen, A11039). Slides were washed once in PBS and incubated in DAPI diluted (1 μg/ ml, Merck) in saline for 5 min. Slides were washed 3x in PBS for 15 min and were mounted with DABCO mounting media.

Super-resolution microscopy

K18-hACE2 mouse brain sections were imaged using an Olympus UPLXAPO 10x/0.4 NA air objective, 20x/0.8 NA air objective and an UPLXAPO 60x/1.42 NA oil-immersion objective mounted on a spinning disk confocal microscope (SpinSR10; Olympus, Japan) built on an Olympus IX3 body equipped with two ORCA-Fusion BT sCMOS cameras (Hamamatsu Photonics K.K., Japan) and controlled by Olympus cellSens software. Images were acquired as

3D Z-stack tile images and were deconvolved using Huygens Professional Deconvolution Software (Scientific Volume Imaging, Netherlands).

RNA-Seq and bioinformatics

In-house RNA-Seq was undertaken as described using Illumina Nextseq 550 platform generating 75 bp paired end reads [46,126]. The per base sequence quality for >90% bases was above Q30 for all samples. Subsequent analyses were undertaken as described [46,126], with the mouse reference genome GRCm39 primary assembly and GENCODE M27 used in the combined reference that included SARS-CoV-2 isolate Wuhan-Hu-1 (NC_045512.2; 29903 bp). In brief, counts for mouse genes and for SARS-CoV-2 were generated using RSEM and differentially expressed genes were determined using EdgeR. To avoid missing type I IFN genes, which have low read counts [131], a low filter of row sum normalized read count >1 was used.

DEGs in direct and indirect interactions were analyzed using Ingenuity Pathway Analysis (IPA) (QIAGEN) using the Canonical pathways, Up-Stream Regulators (USR) and Diseases and Functions features [132].

Statistics

Statistical analyses of experimental data were performed using IBM SPSS Statistics for Windows, Version 19.0 (IBM Corp., Armonk, NY, USA). The t-test was used when the difference in variances was <4, skewness was >-2 and kurtosis was <2. For non-parametric data the Kolmogorov-Smirnov test was used.

Declaration of competing interest

The authors declare that they have no known competing financial interests or personal relationships that could have appeared to influence the work reported in this paper.

Acknowledgements

The authors thank the following QIMRB staff; Dr I. Anraku for management of the PC3 facility at QIMR Berghofer MRI, Dr Viviana Lutzky for proof reading, Crystal Chang, Clay Winterford and Sang-Hee Park for histology services, the animal house staff for mouse breeding and

443 agistment, and Dr. Gunter Hartel for assistance with statistics. The authors gratefully
444 acknowledge the Advanced Microscopy Facility and the Histology Facility at The Queensland
445 Brain Institute for their support and assistance in this work, Dr Rumelo Amor, Dr Arnaud
446 Gaudin, Dr Andrew Thompson.
447
448 **Funding**
449 The authors thank the Brazil Family Foundation (and others) for their generous philanthropic
450 donations that helped set up the PC3 (BSL3) SARS-CoV-2 research facility at QIMR Berghofer
451 MRI, as well as ongoing research into SARS-CoV-2, COVID-19 and long-COVID. A.S. is
452 supported by the National Health and Medical Research Council (NHMRC) of Australia
453 (Investigator grant APP1173880). The funders had no role in study design, data collection and
454 analysis, decision to publish, or preparation of the manuscript. The authors also thank the
455 National Health and Medical Research Council (Project grant APP2010917 to F.A.M.; Senior
456 research Fellowship APP1155794 to F.A.M and the Queensland Research Stimulus Package to
457 F.A.M.
458
459 **Data availability**
460 All data is provided in the manuscript and accompanying supplementary files. Raw sequencing
461 data (fastq files) generated for this publication for RNA-Seq have been deposited in the NCBI
462 SRA, BioProject: PRJNA813692 and are publicly available at the date of publication.
463
464 **Figure Legends**
465
466 **Figure. 1. K18-hACE2 mice infected with an original (ancestral) strain isolate, omicron**
467 **BA.1 and omicron BA.5 isolates. a** Percent weight change post infection. Original ancestral
468 isolate (n=5-12 mice measured per time point), means and SEs are plotted (data from 3
469 independent experiments). BA.1, three mice showed weight loss >20% (requiring euthanasia, †)
470 and are graphed individually; means and SE are plotted for the surviving mice (n=4-15 mice
471 measured per time point). BA.5 (n=6) graphed individually. **b** Disease scores for the indicated
472 overt disease symptoms for animals described in a. For BA.5 the remaining mouse on 6 dpi
473 showed a Posture score of 2. For BA.1 no overt symptoms were seen except in a single animal

on 9 dpi, with this animal one of the 3 that required euthanasia due to weight loss. **c** Kaplan Meyer plot showing percent survival; n=12 for original, n=13 for BA.5 and n=24 for BA.1 (data from 2-3 independent experiments). Statistics by log-rank tests. **d** Viral tissue titers for the indicated organs. Mice were euthanized on the indicated dpi, the indicated organs harvested and the tissue titers determined by $CCID_{50}$ assays. ND – not detected (limit of detection ≈2 $log_{10}CCID_{50}/g$). Bars show means for 5 dpi. Brains BA.1 shows 3 mice that were euthanized due to weight loss (†) and 3 symptom-free mice that were also euthanized at this time point. (Data from 2-3 independent experiments).

Figure 2. Immunohistochemistry of brains of BA.5 infected K18-hACE2 mice using an anti-spike monoclonal antibody. **a** Brain of BA.5-infected K18-hACE2 mouse 6 dpi showing IHC staining in the cortex and hypothalamus. Insert enlargements on the right. **b** As for a showing staining of the hippocampus. Far right shows staining of the axons (arrowheads).

Figure 3. **Histological lesions in brains of BA.5 infected K18-hACE2 mice.** **a** Neuron vacuolation (hydropic degeneration) of neurons (arrowheads) in the cortex 4 dpi. A control brain from mice inoculated with UV-inactivated BA.5 is shown on the right. **b** Perivascular cuffing. A venule (red blood cells in the center) is surrounded by leukocytes (two leukocytes are indicated by arrow heads), 7 dpi. A control venule is shown on the right. **c** Focal vasogenic edema; fluid filled perivascular space (arrowheads), 6 dpi. A control is shown on the right, with arrowheads showing normal perivascular spaces. **d** Microglial nodule; accumulation of microgliocytes (some typical microgliocytes indicated with arrowheads), 6 dpi. **e**. Small hemorrhagic lesion, 7 dpi (arrowheads indicate some extravascular red blood cells).

Figure 4. Neurotropism of Omicron BA.5 in brains of K18-hACE2 mice. K18-hACE2 mice (n=6) were inoculated with omicron BA.5 ($5x10^4$ $CCID_{50}$) and brains collected 5 dpi for histological examination. Brains were fixed, paraffin embedded, sectioned, and stained for SARS-CoV-2 S-protein (red) and DAPI (blue) in conjunction with either the neuronal marker NeuN (green), microglial marker Iba1 (green) or reactive astrocyte maker GFAP (green) using immunofluorescence. **a-c** Representative low magnification 3D Z-stack maximum projections of the cortex of an infected brain section co-stained for S-protein (red) and NeuN (green). Scale bar

= 50 mm. **d-f** Higher magnification image of S-protein in infected neurons (arrowheads indicate infected neurons). Scale bar = 10 mm. (i-ii) Zoom in of infected neurons showing S-protein in vesicle like structures. **g-i** Representative low magnification 3D Z-stack maximum projections of the cortex of an infected brain section co-stained for S-protein (red) and Iba1 (green). Scale bar = 50 mm. **j-l** Higher magnification image showing infected neurons and low levels of S-protein in microglia (arrowheads indicate infected neurons, asterixis indicate microglia with low levels of S-protein). Scale bar = 10 mm. (iii) Zoom in of microglia containing low levels of S-protein. (iv) Zoom in of infected neuron showing microglial processes contacting cells. **m-o** Representative low magnification 3D Z-stack maximum projections of the cortex of an infected brain section stained for S-protein (red) and GFAP (green). Scale bar = 50 mm. **p-r** Higher magnification image showing no reactive astrocytes in region of infection (arrowheads indicate infected neurons). Scale bar = 10 mm. (v) Zoom in of infected neuron with no GFAP.

Figure 5. Transcriptome signatures in brains of K18-hACE2 mice infected with BA.5. RNA-Seq of BA.5 infected brains (n=6) compared with brains of mice inoculated with UV-inactivated BA.5 (n=5) identified 437 DEGs. The DEGs were analyzed by Ingenuity Pathway Analysis (IPA) and GSEAs using the Molecular Signatures Data Base (MSigDB), with a representative sample of annotations shown and grouped by theme (a full list is provided in Supplementary Table 1).

Figure 6. Infection of cortical brain organoids with original ancestral, BA. 1 and BA.5. a IHC of brain organoids 4 dpi with original ancestral and BA.5 using an anti-spike monoclonal antibody. **b** Viral titers in the supernatant of the organoid cultures sampled at the indicated dpi. Statistics by Kolmogorov-Smirnov test. **c** RNA-Seq-derived viral reads counts for infected organoids, 4 dpi. **d** Venn diagram showing overlap of up-regulated DEGs for organoids infected with BA.5 and original ancestral. **e** DEGs (n=2390, $q<0.001$) generated from RNA-Seq of BA.5 infected organoids (n=4) 4 dpi vs uninfected organoids (n=4) were analyzed by IPA. Selected and representative annotations are shown (for full data set see Supplementary Table 2).

References

1 Mallapaty, S. Where did Omicron come from? Three key theories. *Nature* **602**, 26-28 (2022).

2 Du, P., Gao, G. F. & Wang, Q. The mysterious origins of the Omicron variant of SARS-CoV-2. *Innovation (Camb)* **3**, 100206, doi:10.1016/j.xinn.2022.100206 (2022).

3 SARS-CoV-2 sequences by variant, Nov 3, 2022. https://ourworldindata.org/grapher/covid-variants-bar?country=CAN~BWA~ESP~ZAF~AUS~GBR~USA~DEU~ITA~BEL~FRA. (2022).

4 Tanne, J. H. Covid-19: BA.5 variant is now dominant in US as infections rise. *BMJ* **378**, o1770, doi:10.1136/bmj.o1770 (2022).

5 Levine, R. L. Addressing the Long-term Effects of COVID-19. *JAMA* **328**, 823-824, doi:10.1001/jama.2022.14089 (2022).

6 Qasmieh, S. A. *et al.* The prevalence of SARS-CoV-2 infection and long COVID in US adults during the BA.5 surge, June-July 2022. *medRxiv*, 2022.2009.2004.22279588, doi:10.1101/2022.09.04.22279588 (2022).

7 Xu, E., Xie, Y. & Al-Aly, Z. Long-term neurologic outcomes of COVID-19. *Nat Med*, doi:10.1038/s41591-022-02001-z (2022).

8 Monje, M. & Iwasaki, A. The neurobiology of long COVID. *Neuron* **110**, 3484-3496, doi:10.1016/j.neuron.2022.10.006 (2022).

9 Islam, M. A. *et al.* Encephalitis in Patients with COVID-19: A Systematic Evidence-Based Analysis. *Cells* **11**, doi:10.3390/cells11162575 (2022).

10 Ludvigsson, J. F. Convulsions in children with COVID-19 during the Omicron wave. *Acta Paediatr* **111**, 1023-1026, doi:10.1111/apa.16276 (2022).

11 Cloete, J. *et al.* Paediatric hospitalisations due to COVID-19 during the first SARS-CoV-2 omicron (B.1.1.529) variant wave in South Africa: a multicentre observational study. *Lancet Child Adolesc Health* **6**, 294-302, doi:10.1016/S2352-4642(22)00027-X (2022).

12 Taquet, M. *et al.* Neurological and psychiatric risk trajectories after SARS-CoV-2 infection: an analysis of 2-year retrospective cohort studies including 1 284 437 patients. *Lancet Psychiatry* **9**, 815-827, doi:10.1016/S2215-0366(22)00260-7 (2022).

13 Chen, C. S. *et al.* Critical pediatric neurological illness associated with COVID-19 (Omicron BA.2.3.7 variant) infection in Taiwan: immunological assessment and viral genome analysis in tertiary medical center. *Int J Infect Dis* **124**, 45-48, doi:10.1016/j.ijid.2022.09.001 (2022).

14 Hansen, C. H. *et al.* Risk of reinfection, vaccine protection, and severity of infection with the BA.5 omicron subvariant: a nation-wide population-based study in Denmark. *The Lancet Infectious Diseases*, doi:10.1016/S1473-3099(22)00595-3 (2022).

15 Branche, A. R. *et al.* SARS-CoV-2 Variant Vaccine Boosters Trial: Preliminary Analyses. *medRxiv*, doi:10.1101/2022.07.12.22277336 (2022).

16 Surie, D. *et al.* Effectiveness of Monovalent mRNA Vaccines Against COVID-19-Associated Hospitalization Among Immunocompetent Adults During BA.1/BA.2 and BA.4/BA.5 Predominant Periods of SARS-CoV-2 Omicron Variant in the United States - IVY Network, 18 States, December 26, 2021-August 31, 2022. *MMWR Morb Mortal Wkly Rep* **71**, 1327-1334, doi:10.15585/mmwr.mm7142a3 (2022).

17 Takashita, E. *et al.* Efficacy of Antibodies and Antiviral Drugs against Omicron BA.2.12.1, BA.4, and BA.5 Subvariants. *N Engl J Med* **387**, 468-470, doi:10.1056/NEJMc2207519 (2022).

18 Suryawanshi, R. K. *et al.* Limited cross-variant immunity from SARS-CoV-2 Omicron without vaccination. *Nature* **607**, 351-355, doi:10.1038/s41586-022-04865-0 (2022).

19 Bowe, B., Xie, Y. & Al-Aly, Z. Acute and postacute sequelae associated with SARS-CoV-2 reinfection. *Nat Med* **28**, 2398-2405, doi:10.1038/s41591-022-02051-3 (2022).

20 Ledford, H. Severe COVID could cause markers of old age in the brain. *Nature*, doi:10.1038/d41586-022-04253-8 (2022).
21 Graham, E. L., Koralnik, I. J. & Liotta, E. M. Therapeutic Approaches to the Neurologic Manifestations of COVID-19. *Neurotherapeutics* **19**, 1435-1466, doi:10.1007/s13311-022-01267-y (2022).
22 Douaud, G. *et al.* SARS-CoV-2 is associated with changes in brain structure in UK Biobank. *Nature* **604**, 697-707, doi:10.1038/s41586-022-04569-5 (2022).
23 Sanabria-Diaz, G. *et al.* Brain cortical alterations in COVID-19 patients with neurological symptoms. *Front Neurosci* **16**, 992165, doi:10.3389/fnins.2022.992165 (2022).
24 Siow, I., Lee, K. S., Zhang, J. J. Y., Saffari, S. E. & Ng, A. Encephalitis as a neurological complication of COVID-19: A systematic review and meta-analysis of incidence, outcomes, and predictors. *Eur J Neurol* **28**, 3491-3502, doi:10.1111/ene.14913 (2021).
25 Altmayer, V. *et al.* Endothelial cell biomarkers in critically ill COVID-19 patients with encephalitis. *J Neurochem* **161**, 492-505, doi:10.1111/jnc.15545 (2022).
26 Chakraborty, S. & Basu, A. Catching hold of COVID-19-related encephalitis by tracking ANGPTL4 signature in blood: An Editorial Highlight for "Endothelial cell biomarkers in critically ill COVID-19-patients with encephalitis": An Editorial Highlight for "Endothelial cell biomarkers in critically ill COVID-19-patients with encephalitis" on page 492. *J Neurochem* **161**, 458-462, doi:10.1111/jnc.15560 (2022).
27 Samudyata *et al.* SARS-CoV-2 promotes microglial synapse elimination in human brain organoids. *Mol Psychiatry*, doi:10.1038/s41380-022-01786-2 (2022).
28 Zhang, B. Z. *et al.* SARS-CoV-2 infects human neural progenitor cells and brain organoids. *Cell Res* **30**, 928-931, doi:10.1038/s41422-020-0390-x (2020).
29 Aschman, T., Mothes, R., Heppner, F. L. & Radbruch, H. What SARS-CoV-2 does to our brains. *Immunity* **55**, 1159-1172, doi:https://doi.org/10.1016/j.immuni.2022.06.013 (2022).
30 Bauer, L. *et al.* The neuroinvasiveness, neurotropism, and neurovirulence of SARS-CoV-2. *Trends Neurosci* **45**, 358-368, doi:10.1016/j.tins.2022.02.006 (2022).
31 Rutkai, I. *et al.* Neuropathology and virus in brain of SARS-CoV-2 infected non-human primates. *Nat Commun* **13**, 1745, doi:10.1038/s41467-022-29440-z (2022).
32 Andrews, M. G. *et al.* Tropism of SARS-CoV-2 for human cortical astrocytes. *Proc Natl Acad Sci U S A* **119**, e2122236119, doi:10.1073/pnas.2122236119 (2022).
33 Stein, S. R. *et al.* SARS-CoV-2 infection and persistence in the human body and brain at autopsy. *Nature*, doi:10.1038/s41586-022-05542-y (2022).
34 Crunfli, F. *et al.* Morphological, cellular, and molecular basis of brain infection in COVID-19 patients. *Proc Natl Acad Sci U S A* **119**, e2200960119, doi:10.1073/pnas.2200960119 (2022).
35 Bulfamante, G. *et al.* First ultrastructural autoptic findings of SARS -Cov-2 in olfactory pathways and brainstem. *Minerva Anestesiol* **86**, 678-679, doi:10.23736/S0375-9393.20.14772-2 (2020).
36 Shen, W. B. *et al.* SARS-CoV-2 invades cognitive centers of the brain and induces Alzheimer's-like neuropathology. *bioRxiv*, doi:10.1101/2022.01.31.478476 (2022).
37 Song, E. *et al.* Neuroinvasion of SARS-CoV-2 in human and mouse brain. *J Exp Med* **218**, doi:10.1084/jem.20202135 (2021).
38 Matschke, J. *et al.* Neuropathology of patients with COVID-19 in Germany: a post-mortem case series. *Lancet Neurol* **19**, 919-929, doi:10.1016/S1474-4422(20)30308-2 (2020).
39 Serrano, G. E. *et al.* SARS-CoV-2 Brain Regional Detection, Histopathology, Gene Expression, and Immunomodulatory Changes in Decedents with COVID-19. *J Neuropathol Exp Neurol* **81**, 666-695, doi:10.1093/jnen/nlac056 (2022).
40 Elmakaty, I. *et al.* Clinical Implications of COVID-19 Presence in CSF: Systematic Review of Case Reports. *Cells* **11**, doi:10.3390/cells11203212 (2022).

41 Abdolahi, S., Ashayeri Ahmadabad, R., Gorji, A. & Mirzaasgari, Z. Status epilepticus and the presence of SARS-COV-2 in the cerebrospinal fluid: A case report. *Clin Case Rep* **10**, e6214, doi:10.1002/ccr3.6214 (2022).

42 Ayuningtyas, T., Natadidjaja, R. I., Octaviani, C., Sahli, F. & Adlani, H. Confirmed severe acute respiratory syndrome coronavirus 2 encephalitis in cerebrospinal fluid: a case report. *J Med Case Rep* **16**, 154, doi:10.1186/s13256-022-03376-w (2022).

43 Viszlayova, D. *et al.* SARS-CoV-2 RNA in the Cerebrospinal Fluid of a Patient with Long COVID. *Ther Adv Infect Dis* **8**, 20499361211048572, doi:10.1177/20499361211048572 (2021).

44 Luis, M. B., Liguori, N. F., Lopez, P. A. & Alonso, R. SARS-CoV-2 RNA detection in cerebrospinal fluid: Presentation of two cases and review of literature. *Brain Behav Immun Health* **15**, 100282, doi:10.1016/j.bbih.2021.100282 (2021).

45 Dang, T. Q., La, D. T. & Tran, T. N. Myeloencephalitis as the only presentation of Omicron SARS-CoV-2 infection. *BMJ Case Rep* **15**, doi:10.1136/bcr-2022-251922 (2022).

46 Bishop, C. R. *et al.* Mouse models of COVID-19 recapitulate inflammatory pathways rather than gene expression. *PLoS Pathog* **18**, e1010867, doi:10.1371/journal.ppat.1010867 (2022).

47 Yinda, C. K. *et al.* K18-hACE2 mice develop respiratory disease resembling severe COVID-19. *PLoS Pathog* **17**, e1009195, doi:10.1371/journal.ppat.1009195 (2021).

48 Dong, W. *et al.* The K18-Human ACE2 Transgenic Mouse Model Recapitulates Non-severe and Severe COVID-19 in Response to an Infectious Dose of the SARS-CoV-2 Virus. *J Virol* **96**, e0096421, doi:10.1128/JVI.00964-21 (2022).

49 Vidal, E. *et al.* Chronological brain lesions after SARS-CoV-2 infection in hACE2-transgenic mice. *Vet Pathol* **59**, 613-626, doi:10.1177/03009858211066841 (2022).

50 Rothan, H. A. *et al.* SARS-CoV-2 Infects Primary Neurons from Human ACE2 Expressing Mice and Upregulates Genes Involved in the Inflammatory and Necroptotic Pathways. *Pathogens* **11**, doi:10.3390/pathogens11020257 (2022).

51 Olivarria Gema, M. *et al.* Microglia Do Not Restrict SARS-CoV-2 Replication following Infection of the Central Nervous System of K18-Human ACE2 Transgenic Mice. *Journal of Virology* **96**, e01969-01921, doi:10.1128/jvi.01969-21 (2022).

52 Carossino, M. *et al.* Fatal Neurodissemination and SARS-CoV-2 Tropism in K18-hACE2 Mice Is Only Partially Dependent on hACE2 Expression. *Viruses* **14** (2022).

53 Dumenil, T. *et al.* Warmer ambient air temperatures reduce nasal turbinate and brain infection, but increase lung inflammation in the K18-hACE2 mouse model of COVID-19. *Sci Total Environ* **859**, 160163, doi:10.1016/j.scitotenv.2022.160163 (2022).

54 Morgan, M. S. *et al.* Monoclonal antibodies specific for SARS-CoV-2 spike protein suitable for multiple applications for current variants of concern. *Viruses* **(in press** (2022).

55 Meinhardt, J. *et al.* Olfactory transmucosal SARS-CoV-2 invasion as a port of central nervous system entry in individuals with COVID-19. *Nat Neurosci* **24**, 168-175, doi:10.1038/s41593-020-00758-5 (2021).

56 Awogbindin, I. O. *et al.* Microglial Implications in SARS-CoV-2 Infection and COVID-19: Lessons From Viral RNA Neurotropism and Possible Relevance to Parkinson's Disease. *Front Cell Neurosci* **15**, 670298, doi:10.3389/fncel.2021.670298 (2021).

57 Beckman, D. *et al.* SARS-CoV-2 infects neurons and induces neuroinflammation in a non-human primate model of COVID-19. *Cell Rep* **41**, 111573, doi:10.1016/j.celrep.2022.111573 (2022).

58 Seehusen, F. *et al.* Neuroinvasion and Neurotropism by SARS-CoV-2 Variants in the K18-hACE2 Mouse. *Viruses* **14**, doi:10.3390/v14051020 (2022).

59 Ferren, M. *et al.* Hamster organotypic modeling of SARS-CoV-2 lung and brainstem infection. *Nat Commun* **12**, 5809, doi:10.1038/s41467-021-26096-z (2021).

60 Tarres-Freixas, F. *et al.* Heterogeneous Infectivity and Pathogenesis of SARS-CoV-2 Variants Beta, Delta and Omicron in Transgenic K18-hACE2 and Wildtype Mice. *Front Microbiol* **13**, 840757, doi:10.3389/fmicb.2022.840757 (2022).

61 Halfmann, P. J. *et al.* SARS-CoV-2 Omicron virus causes attenuated disease in mice and hamsters. *Nature* **603**, 687-692, doi:10.1038/s41586-022-04441-6 (2022).

62 Shuai, H. *et al.* Attenuated replication and pathogenicity of SARS-CoV-2 B.1.1.529 Omicron. *Nature* **603**, 693-699, doi:10.1038/s41586-022-04442-5 (2022).

63 Uraki, R. *et al.* Characterization of SARS-CoV-2 Omicron BA.4 and BA.5 isolates in rodents. *Nature*, doi:10.1038/s41586-022-05482-7 (2022).

64 Rizvi, Z. A. *et al.* Omicron sub-lineage BA.5 infection causes attenuated pathology and results in robust protection in Omicron recovered hACE2 transgenic mice. Available at SSRN: https://ssrn.com/abstract=4243698 or http://dx.doi.org/10.2139/ssrn.4243698. (2022).

65 Shrestha, L. B., Foster, C., Rawlinson, W., Tedla, N. & Bull, R. A. Evolution of the SARS-CoV-2 omicron variants BA.1 to BA.5: Implications for immune escape and transmission. *Rev Med Virol* **32**, e2381, doi:10.1002/rmv.2381 (2022).

66 Sigal, A. Milder disease with Omicron: is it the virus or the pre-existing immunity? *Nat Rev Immunol* **22**, 69-71, doi:10.1038/s41577-022-00678-4 (2022).

67 Chen, D. Y. *et al.* Role of spike in the pathogenic and antigenic behavior of SARS-CoV-2 BA.1 Omicron. *bioRxiv*, doi:10.1101/2022.10.13.512134 (2022).

68 Guo, K. *et al.* Interferon resistance of emerging SARS-CoV-2 variants. *Proc Natl Acad Sci U S A* **119**, e2203760119, doi:10.1073/pnas.2203760119 (2022).

69 Rashid, F. *et al.* Roles and functions of SARS-CoV-2 proteins in host immune evasion. *Front Immunol* **13**, 940756, doi:10.3389/fimmu.2022.940756 (2022).

70 Wolter, N. *et al.* Clinical severity of SARS-CoV-2 Omicron BA.4 and BA.5 lineages compared to BA.1 and Delta in South Africa. *Nat Commun* **13**, 5860, doi:10.1038/s41467-022-33614-0 (2022).

71 Mesci, P. *et al.* SARS-CoV-2 infects human brain organoids causing cell death and loss of synapses that can be rescued by treatment with Sofosbuvir. *PLOS Biology* **20**, e3001845, doi:10.1371/journal.pbio.3001845 (2022).

72 Kong, W. *et al.* Neuropilin-1 Mediates SARS-CoV-2 Infection of Astrocytes in Brain Organoids, Inducing Inflammation Leading to Dysfunction and Death of Neurons. *mBio* **0**, e02308-02322, doi:10.1128/mbio.02308-22 (2022).

73 Hou, Y. *et al.* Enhanced replication of SARS-CoV-2 Omicron BA.2 in human forebrain and midbrain organoids. *Signal Transduction and Targeted Therapy* **7**, 381, doi:10.1038/s41392-022-01241-2 (2022).

74 Callaway, E. Will there be a COVID winter wave? What scientists say. *Nature* **610**, 239-241, doi:10.1038/d41586-022-03157-x (2022).

75 Barut, G. T. *et al.* The spike gene is a major determinant for the SARS-CoV-2 Omicron-BA.1 phenotype. *Nat Commun* **13**, 5929, doi:10.1038/s41467-022-33632-y (2022).

76 Oh, S.-J. & Shin, O. S. SARS-CoV-2-mediated evasion strategies for antiviral interferon pathways. *Journal of Microbiology* **60**, 290-299, doi:10.1007/s12275-022-1525-1 (2022).

77 Zheng, J. *et al.* COVID-19 treatments and pathogenesis including anosmia in K18-hACE2 mice. *Nature* **589**, 603-607, doi:10.1038/s41586-020-2943-z (2021).

78 Kumari, P. *et al.* Neuroinvasion and Encephalitis Following Intranasal Inoculation of SARS-CoV-2 in K18-hACE2 Mice. *Viruses* **13**, 132, doi:10.3390/v13010132 (2021).

79 Yu, P. *et al.* Comparative pathology of the nasal epithelium in K18-hACE2 Tg mice, hACE2 Tg mice, and hamsters infected with SARS-CoV-2. *Vet Pathol*, 3009858211071016, doi:10.1177/03009858211071016 (2022).

80 Amarilla, A. A. *et al.* A versatile reverse genetics platform for SARS-CoV-2 and other positive-strand RNA viruses. *Nat Commun* **12**, 3431, doi:10.1038/s41467-021-23779-5 (2021).

81 Bauer, L. *et al.* In vitro and in vivo differences in neurovirulence between D614G, Delta And Omicron BA.1 SARS-CoV-2 variants. *Acta Neuropathologica Communications* **10**, 124, doi:10.1186/s40478-022-01426-4 (2022).

82 Radhakrishnan, R. K. & Kandasamy, M. SARS-CoV-2-Mediated Neuropathogenesis, Deterioration of Hippocampal Neurogenesis and Dementia. *Am J Alzheimers Dis Other Demen* **37**, 15333175221078418, doi:10.1177/15333175221078418 (2022).

83 Paul, T. *et al.* Adrenal tropism of SARS-CoV-2 and adrenal findings in a post-mortem case series of patients with severe fatal COVID-19. *Nat Commun* **13**, 1589, doi:10.1038/s41467-022-29145-3 (2022).

84 Bellastella, G. *et al.* Neuroimmunoendocrinology of SARS-CoV 2 Infection. *Biomedicines* **10**, doi:10.3390/biomedicines10112855 (2022).

85 Bullen, C. K. *et al.* Infectability of human BrainSphere neurons suggests neurotropism of SARS-CoV-2. *ALTEX* **37**, 665-671, doi:10.14573/altex.2006111 (2020).

86 Fumagalli, V. *et al.* Administration of aerosolized SARS-CoV-2 to K18-hACE2 mice uncouples respiratory infection from fatal neuroinvasion. *Sci Immunol* **7**, eabl9929, doi:10.1126/sciimmunol.abl9929 (2022).

87 Rosu, G. C. *et al.* Subtle vascular and astrocytic changes in the brain of coronavirus disease 2019 (COVID-19) patients. *Eur J Neurol* **29**, 3676-3692, doi:10.1111/ene.15545 (2022).

88 Schwabenland, M. *et al.* Deep spatial profiling of human COVID-19 brains reveals neuroinflammation with distinct microanatomical microglia-T-cell interactions. *Immunity* **54**, 1594-1610 e1511, doi:10.1016/j.immuni.2021.06.002 (2021).

89 Pajo, A. T., Espiritu, A. I., Apor, A. & Jamora, R. D. G. Neuropathologic findings of patients with COVID-19: a systematic review. *Neurol Sci* **42**, 1255-1266, doi:10.1007/s10072-021-05068-7 (2021).

90 Maiese, A. *et al.* SARS-CoV-2 and the brain: A review of the current knowledge on neuropathology in COVID-19. *Brain Pathol* **31**, e13013, doi:10.1111/bpa.13013 (2021).

91 Martin, M. *et al.* Postmortem brain 7T MRI with minimally invasive pathological correlation in deceased COVID-19 subjects. *Insights Imaging* **13**, 7, doi:10.1186/s13244-021-01144-w (2022).

92 Al-Dalahmah, O. *et al.* Neuronophagia and microglial nodules in a SARS-CoV-2 patient with cerebellar hemorrhage. *Acta Neuropathol Commun* **8**, 147, doi:10.1186/s40478-020-01024-2 (2020).

93 Mukerji, S. S. & Solomon, I. H. What can we learn from brain autopsies in COVID-19? *Neurosci Lett* **742**, 135528, doi:10.1016/j.neulet.2020.135528 (2021).

94 Bellucci, G. *et al.* Multiple Sclerosis and SARS-CoV-2: Has the Interplay Started? *Front Immunol* **12**, 755333, doi:10.3389/fimmu.2021.755333 (2021).

95 Ismail, II & Salama, S. Association of CNS demyelination and COVID-19 infection: an updated systematic review. *J Neurol* **269**, 541-576, doi:10.1007/s00415-021-10752-x (2022).

96 Sepehrinezhad, A., Gorji, A. & Sahab Negah, S. SARS-CoV-2 may trigger inflammasome and pyroptosis in the central nervous system: a mechanistic view of neurotropism. *Inflammopharmacology* **29**, 1049-1059, doi:10.1007/s10787-021-00845-4 (2021).

97 Rawle, D. J. *et al.* Microplastic consumption induces inflammatory signatures in the colon and prolongs a viral arthritis. *Sci Total Environ* **809**, 152212, doi:10.1016/j.scitotenv.2021.152212 (2022).

98 Durante, M. A. *et al.* Single-cell analysis of olfactory neurogenesis and differentiation in adult humans. *Nat Neurosci* **23**, 323-326, doi:10.1038/s41593-020-0587-9 (2020).

99 Serafini, R. A. *et al.* SARS-CoV-2 Airway Infection Results in Time-dependent Sensory Abnormalities in a Hamster Model. *bioRxiv*, doi:10.1101/2022.08.19.504551 (2022).
100 Banerjee, A. K. *et al.* SARS-CoV-2 Disrupts Splicing, Translation, and Protein Trafficking to Suppress Host Defenses. *Cell* **183**, 1325-1339 e1321, doi:10.1016/j.cell.2020.10.004 (2020).
101 Schmidt, N. *et al.* The SARS-CoV-2 RNA–protein interactome in infected human cells. *Nature Microbiology* **6**, 339-353, doi:10.1038/s41564-020-00846-z (2021).
102 Oner, E. *et al.* Investigation of berberine and its derivatives in Sars Cov-2 main protease structure by molecular docking, PROTOX-II and ADMET methods: in machine learning and in silico study. *J Biomol Struct Dyn*, 1-16, doi:10.1080/07391102.2022.2142848 (2022).
103 Tian, M. *et al.* HIF-1alpha promotes SARS-CoV-2 infection and aggravates inflammatory responses to COVID-19. *Signal Transduct Target Ther* **6**, 308, doi:10.1038/s41392-021-00726-w (2021).
104 Tamura, T. *et al.* Comparative pathogenicity of SARS-CoV-2 Omicron subvariants including BA.1, BA.2, and BA.5. *bioRxiv*, 2022.2008.2005.502758, doi:10.1101/2022.08.05.502758 (2022).
105 Ong, C. P. *et al.* Comparative analysis of SARS-CoV-2 Omicron BA.2.12.1 and BA.5.2 variants. *Journal of Medical Virology* **95**, e28326, doi:https://doi.org/10.1002/jmv.28326 (2023).
106 Aggarwal, A. *et al.* SARS-CoV-2 Omicron BA.5: Evolving tropism and evasion of potent humoral responses and resistance to clinical immunotherapeutics relative to viral variants of concern. *eBioMedicine* **84**, 104270, doi:https://doi.org/10.1016/j.ebiom.2022.104270 (2022).
107 Meng, B. *et al.* Altered TMPRSS2 usage by SARS-CoV-2 Omicron impacts infectivity and fusogenicity. *Nature* **603**, 706-714, doi:10.1038/s41586-022-04474-x (2022).
108 Zhao, H. *et al.* SARS-CoV-2 Omicron variant shows less efficient replication and fusion activity when compared with Delta variant in TMPRSS2-expressed cells. *Emerging Microbes & Infections* **11**, 277-283, doi:10.1080/22221751.2021.2023329 (2022).
109 Abbasi, A. Z. *et al.* Spiking dependence of SARS-CoV-2 pathogenicity on TMPRSS2. *Journal of Medical Virology* **93**, 4205-4218, doi:https://doi.org/10.1002/jmv.26911 (2021).
110 Iwata-Yoshikawa, N. *et al.* Essential role of TMPRSS2 in SARS-CoV-2 infection in murine airways. *Nature Communications* **13**, 6100, doi:10.1038/s41467-022-33911-8 (2022).
111 Li, K., Meyerholz David, K., Bartlett Jennifer, A. & McCray Paul, B. The TMPRSS2 Inhibitor Nafamostat Reduces SARS-CoV-2 Pulmonary Infection in Mouse Models of COVID-19. *mBio* **12**, e00970-00921, doi:10.1128/mBio.00970-21 (2021).
112 Fodoulian, L. *et al.* SARS-CoV-2 Receptors and Entry Genes Are Expressed in the Human Olfactory Neuroepithelium and Brain. *iScience* **23**, 101839, doi:https://doi.org/10.1016/j.isci.2020.101839 (2020).
113 Vu, M. N. *et al.* QTQTN motif upstream of the furin-cleavage site plays a key role in SARS-CoV-2 infection and pathogenesis. *Proceedings of the National Academy of Sciences* **119**, e2205690119, doi:10.1073/pnas.2205690119 (2022).
114 Peacock, T. P. *et al.* The furin cleavage site in the SARS-CoV-2 spike protein is required for transmission in ferrets. *Nature Microbiology* **6**, 899-909, doi:10.1038/s41564-021-00908-w (2021).
115 Lemmin, T., Kalbermatter, D., Harder, D., Plattet, P. & Fotiadis, D. Structures and dynamics of the novel S1/S2 protease cleavage site loop of the SARS-CoV-2 spike glycoprotein. *Journal of Structural Biology: X* **4**, 100038, doi:https://doi.org/10.1016/j.yjsbx.2020.100038 (2020).
116 Frere, J. J. *et al.* SARS-CoV-2 infection in hamsters and humans results in lasting and unique systemic perturbations after recovery. *Science Translational Medicine* **14**, eabq3059, doi:10.1126/scitranslmed.abq3059.
117 Papa, G. *et al.* Furin cleavage of SARS-CoV-2 Spike promotes but is not essential for infection and cell-cell fusion. *PLOS Pathogens* **17**, e1009246, doi:10.1371/journal.ppat.1009246 (2021).

118 Geoghegan, J. L. & Holmes, E. C. The phylogenomics of evolving virus virulence. *Nat Rev Genet* **19**, 756-769, doi:10.1038/s41576-018-0055-5 (2018).

119 Telenti, A., Hodcroft, E. B. & Robertson, D. L. The Evolution and Biology of SARS-CoV-2 Variants. *Cold Spring Harb Perspect Med* **12**, doi:10.1101/cshperspect.a041390 (2022).

120 Wymant, C. *et al.* A highly virulent variant of HIV-1 circulating in the Netherlands. *Science* **375**, 540-545, doi:10.1126/science.abk1688 (2022).

121 Elsworth, P. *et al.* Increased virulence of rabbit haemorrhagic disease virus associated with genetic resistance in wild Australian rabbits (Oryctolagus cuniculus). *Virology* **464-465**, 415-423, doi:10.1016/j.virol.2014.06.037 (2014).

122 Kerr, P. J. *et al.* Next step in the ongoing arms race between myxoma virus and wild rabbits in Australia is a novel disease phenotype. *Proc Natl Acad Sci U S A* **114**, 9397-9402, doi:10.1073/pnas.1710336114 (2017).

123 RADC. in *Alzheimer's Association International Conference* (https://aaic.alz.org/downloads2022/COVID-and-Cognition-News-Release-AAIC2022.pdf, San Diego, 2022).

124 Cantuti-Castelvetri, L. *et al.* Neuropilin-1 facilitates SARS-CoV-2 cell entry and infectivity. *Science* **370**, 856-860, doi:10.1126/science.abd2985 (2020).

125 Pelizzari, L. *et al.* Mid-term MRI evaluation reveals microstructural white matter alterations in COVID-19 fully recovered subjects with anosmia presentation. *Ther Adv Neurol Disord* **15**, 17562864221111995, doi:10.1177/17562864221111995 (2022).

126 Rawle, D. J. *et al.* ACE2-lentiviral transduction enables mouse SARS-CoV-2 infection and mapping of receptor interactions. *PLoS Pathog* **17**, e1009723, doi:10.1371/journal.ppat.1009723 (2021).

127 Yan, K. *et al.* Evolution of ACE2-independent SARS-CoV-2 infection and mouse adaption after passage in cells expressing human and mouse ACE2. *Virus Evol* **8**, veac063, doi:10.1093/ve/veac063 (2022).

128 Yan, K., Rawle, D. J., Le, T. T. & Suhrbier, A. Simple rapid in vitro screening method for SARS-CoV-2 anti-virals that identifies potential cytomorbidity-associated false positives. *Virol J* **18**, 123, doi:10.1186/s12985-021-01587-z (2021).

129 The Jackson Laboratory. B6.Cg-Tg(K18-ACE2)2Prlmn/J. Protocol 38275. https://www.jax.org/Protocol?stockNumber=034860&protocolID=38275.

130 Oikari, L. E. *et al.* Altered Brain Endothelial Cell Phenotype from a Familial Alzheimer Mutation and Its Potential Implications for Amyloid Clearance and Drug Delivery. *Stem Cell Reports* **14**, 924-939, doi:10.1016/j.stemcr.2020.03.011 (2020).

131 Wilson, J. A. C. *et al.* RNA-Seq analysis of chikungunya virus infection and identification of granzyme A as a major promoter of arthritic inflammation. *PLOS Pathogens* **13**, e1006155, doi:10.1371/journal.ppat.1006155 (2017).

132 Rawle, D. J. *et al.* Widespread discrepancy in Nnt genotypes and genetic backgrounds complicates granzyme A and other knockout mouse studies. *Elife* **11**, doi:10.7554/eLife.70207 (2022).

Figure 1

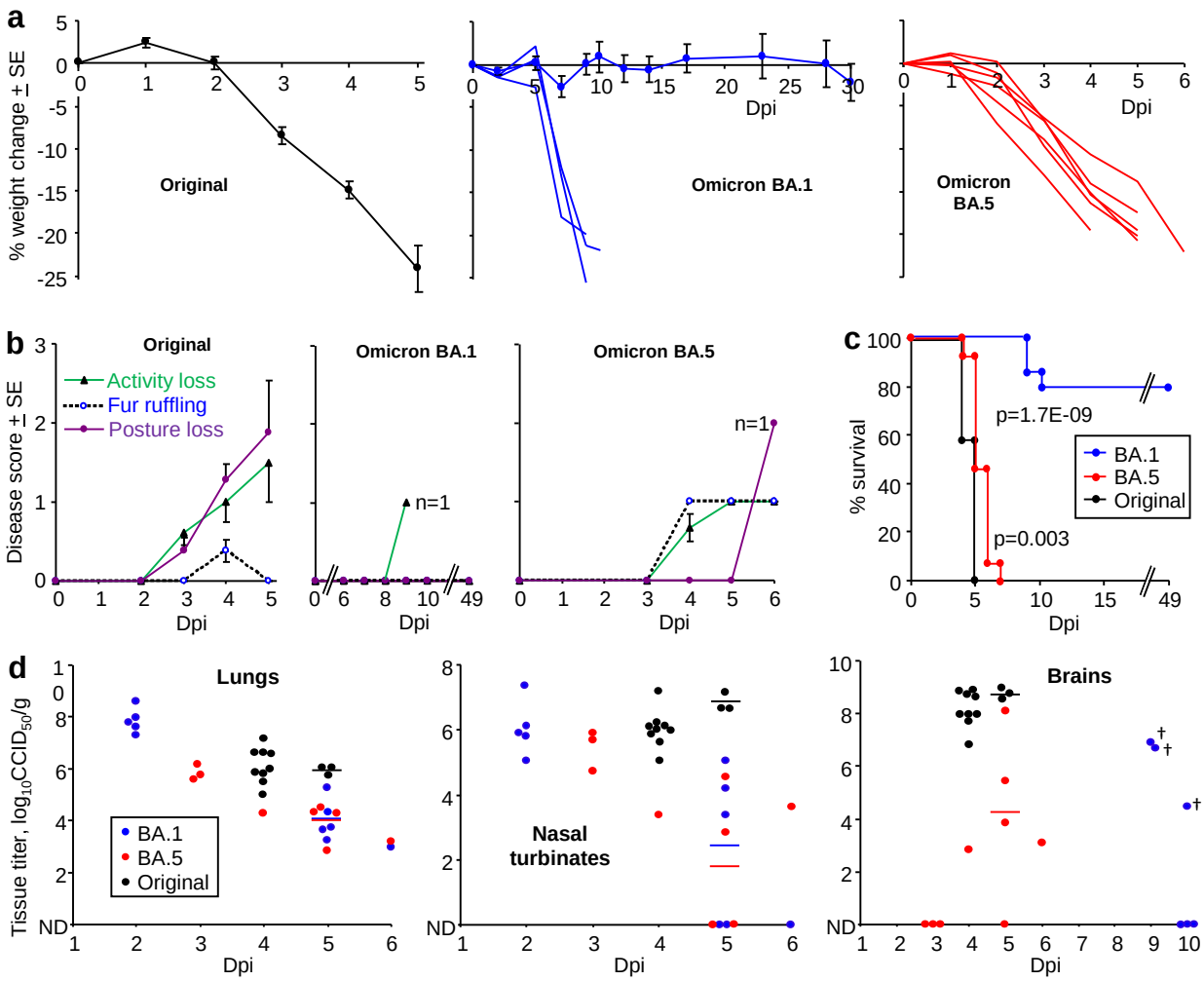

Figure 2

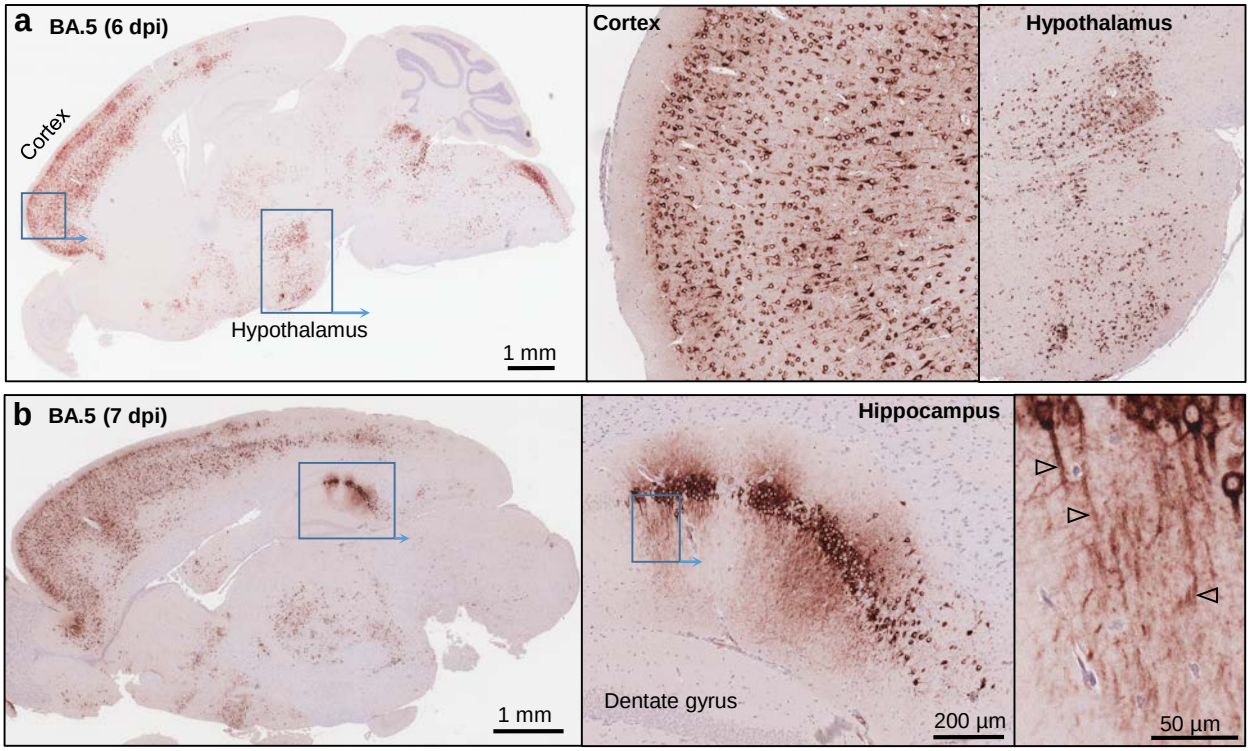

Figure 3

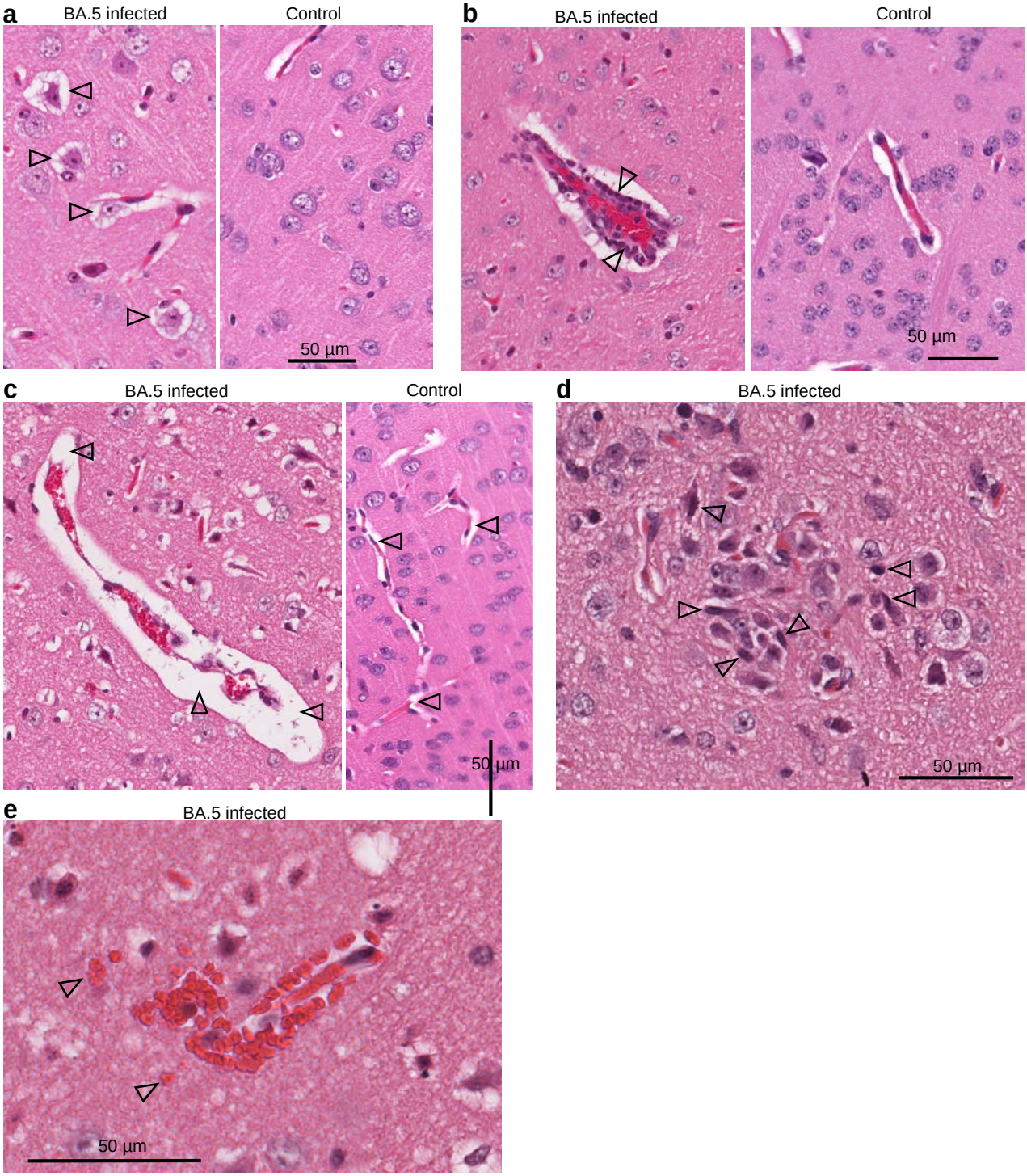

Figure 4

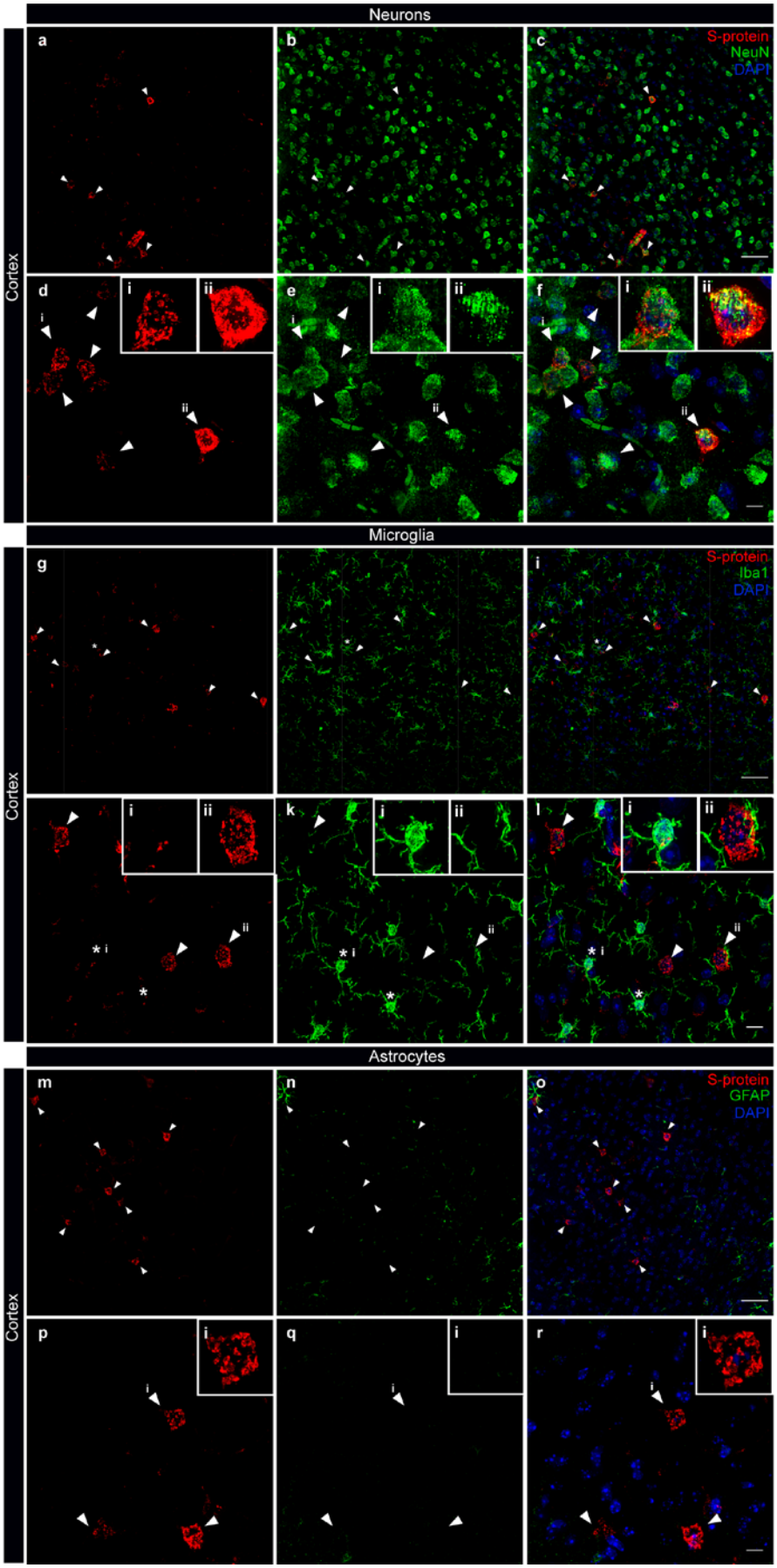

Figure 5

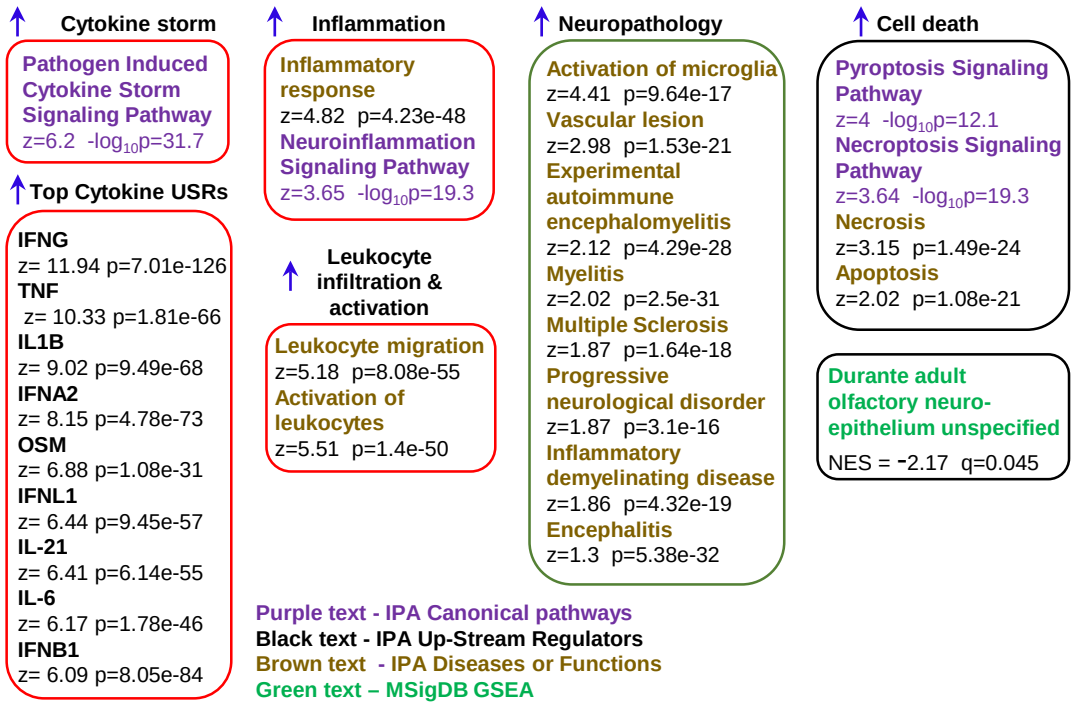

Figure 6

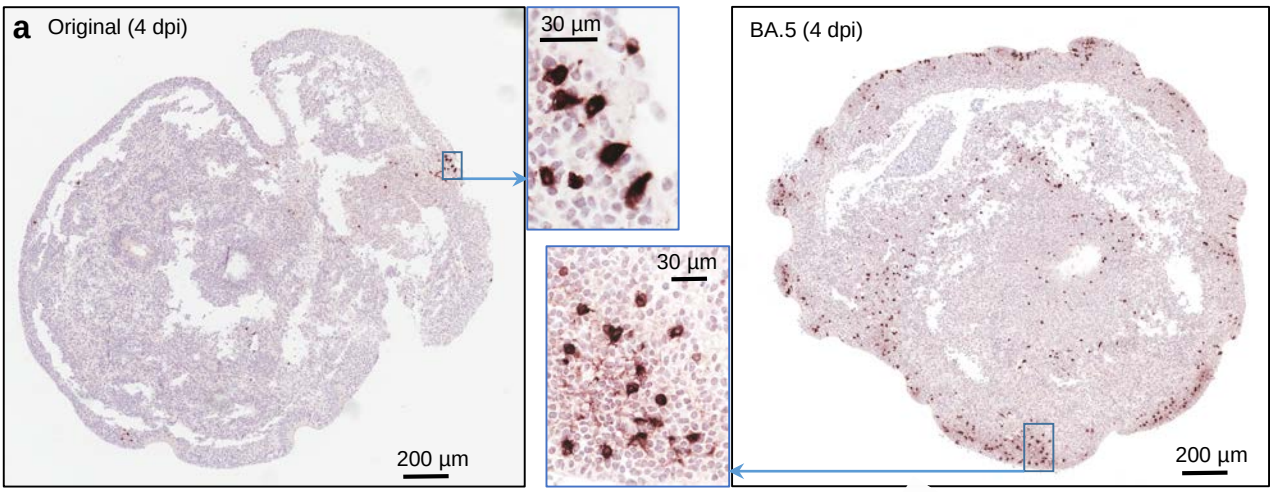

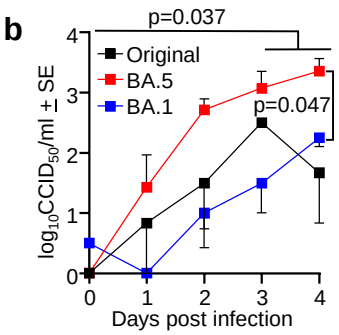

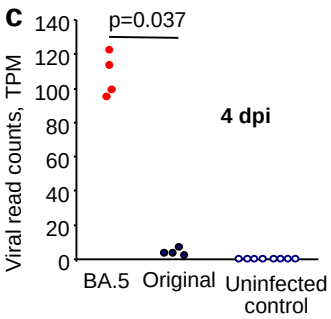

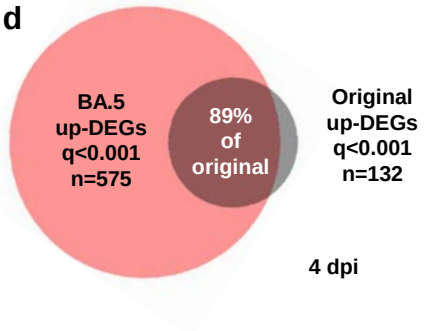

e

Viral pathology

Coronavirus Pathogenesis Pathway
z=1.76 -log10p=5.1

Top USRs

PTPRR
z=6.32 p=1.85e-16
COPS5
z= 6.18 p= p=4.55e-16
LARP1
z= 5 p= p=5.72e-08
ESR1
z= 4.9 p=8.84e-09
EGLN
z= 4.7 p= p=2.94e-03

Neuropathology

Motor dysfunction or movement disorder
z=4.23 p=1.28e-06
Neural tube defect
z=3.86 p=2.17e-09
Congenital neurological disorder
z=3.77 p=2.72e-20
Early-onset encephalopathy
z=2.71 p=2.16e-14

Disruption of neurons

Proliferation of neuronal cells
z= -3.99 p=4.56e-09
Development of neurons
z= -3.66 p=4.57e-17
Migration of neurons
z= -2.48 p=4.61e-06
Quantity of neurons
z= -1.95 p=2.56e-08

Cell death

Organismal death
z=13.43 p=4.02e-27
Apoptosis
z=2.77 p=2.39e-19
Necrosis
z=2.68 p=1.99e-24
Neuronal cell death
z=1.6 p=2.31e-10

Purple text - IPA Canonical pathways
Black text - IPA Up-Stream Regulators
Brown text - IPA Diseases or Functions

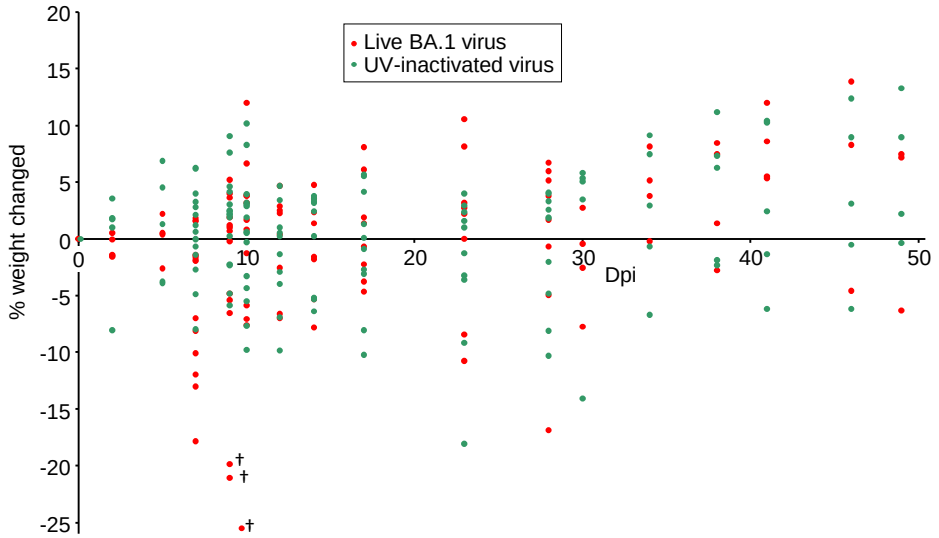

Supplementary Fig. 1. **a** Expanded data for Fig. 1a showing all weight measurements. There were n=24 mice in total infected with BA.1 and n=25 mice inoculated with UV-inactivated BA.1. Some mice were euthanized at specific time points to assess tissue titers (Fig. 1d), others n=3 (†), were euthanized as they reach the ethically defined end point (>20% weight loss). Note that inoculation with UV-inactivated virus (at the same protein dose as live virus) by itself causes weight loss, although usually <15%.

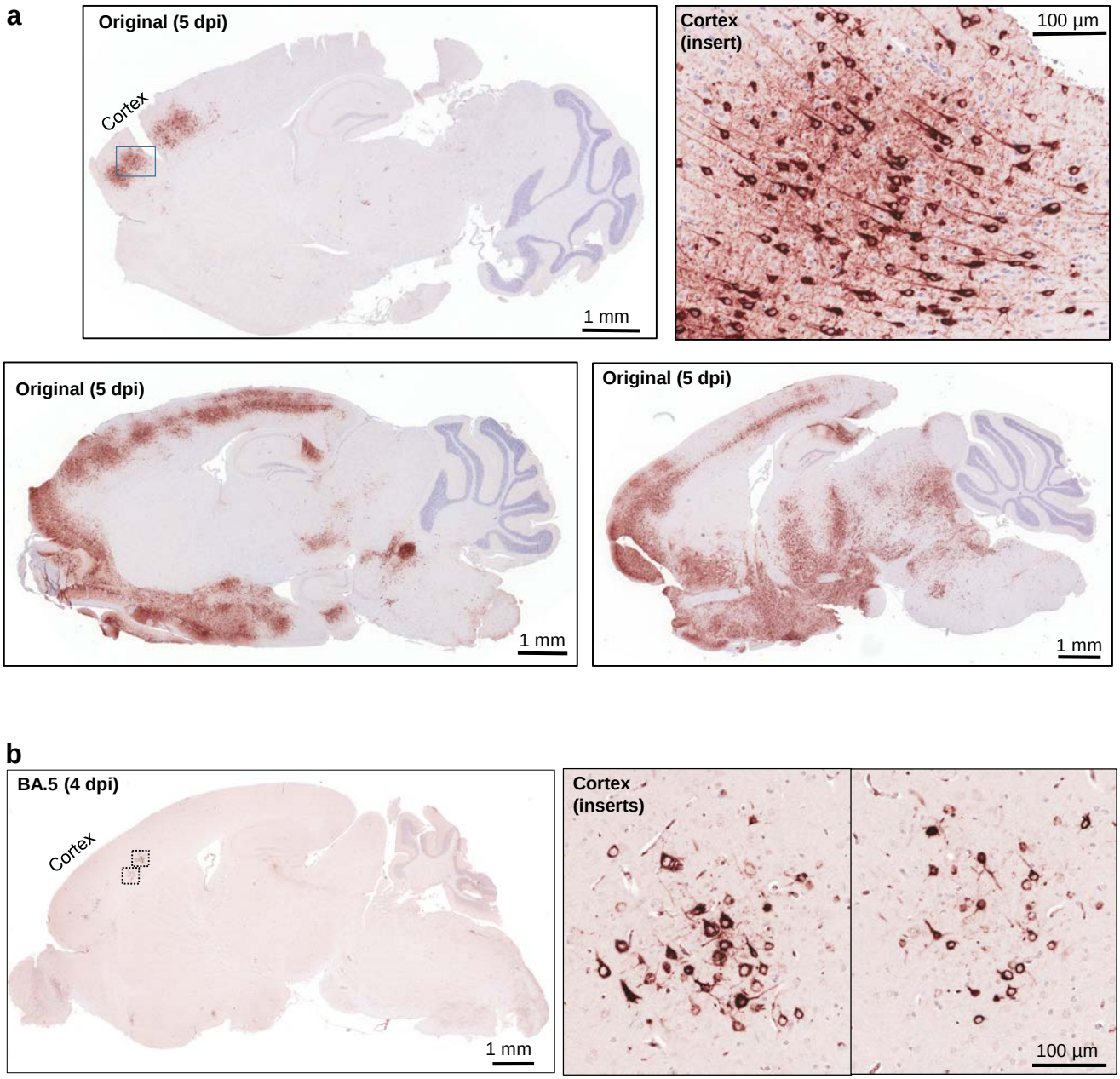

Supplementary Fig. 2. Anti-spike monoclonal antibody straining of brains by immuno-histochemistry (IHC). **a** IHC of brains from K18-hACE2 mice infected with original strain isolate, illustrating the range of IHC staining. Top right shows an enlarged image from the cortex indicating infection of neurons. **b** As for a but infection with omicron BA.5. Despite relatively low level of IHC staining in the brain this mouse reached ethically defined endpoint requiring euthanasia by day 4.

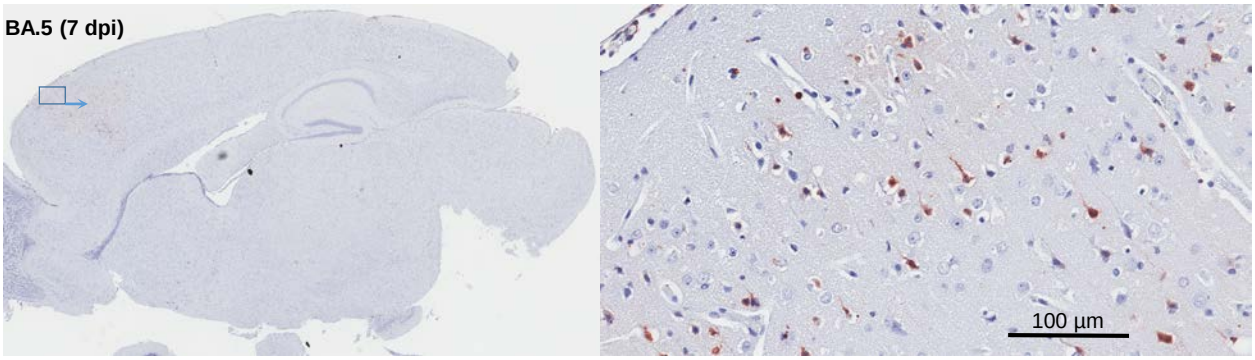

Supplementary Fig. 3. Apotag staining of the brain shown in Fig. 2b. Insert shown on the right.

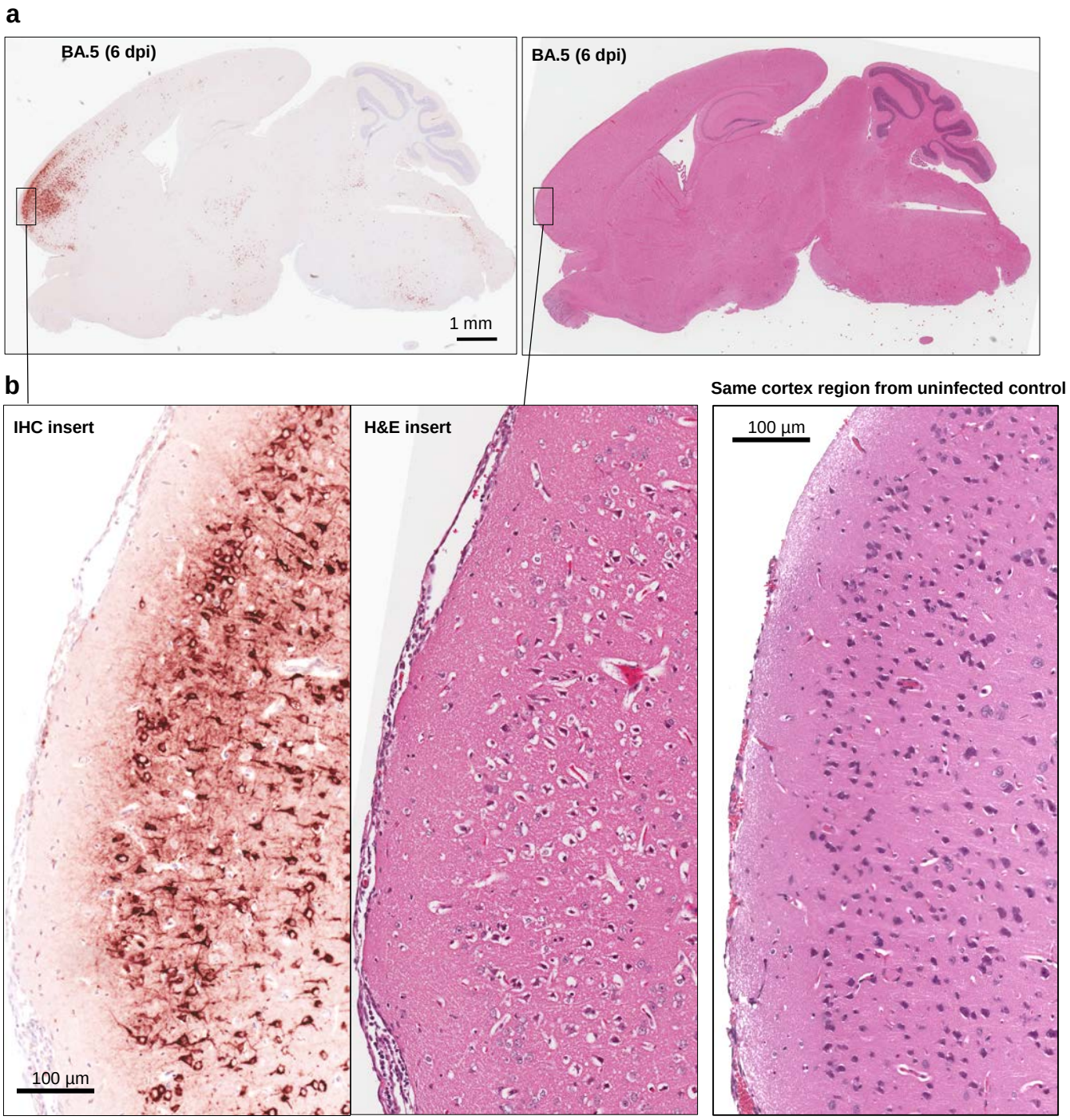

Supplementary Fig. 4. **a** Anti-spike monoclonal antibody straining by immuno-histochemistry (IHC) of brain from a BA.5 infected K18-hACE2 mouse (left) and H&E staining of a section from the same block (right). **b** Inserts showing association of viral antigen detection in the cortex (IHC positive staining) with high density of H&E lesions (primarily vacuolation). A control is shown bottom right; H&E staiing of the same region of the cortex in a control uninfected animal.

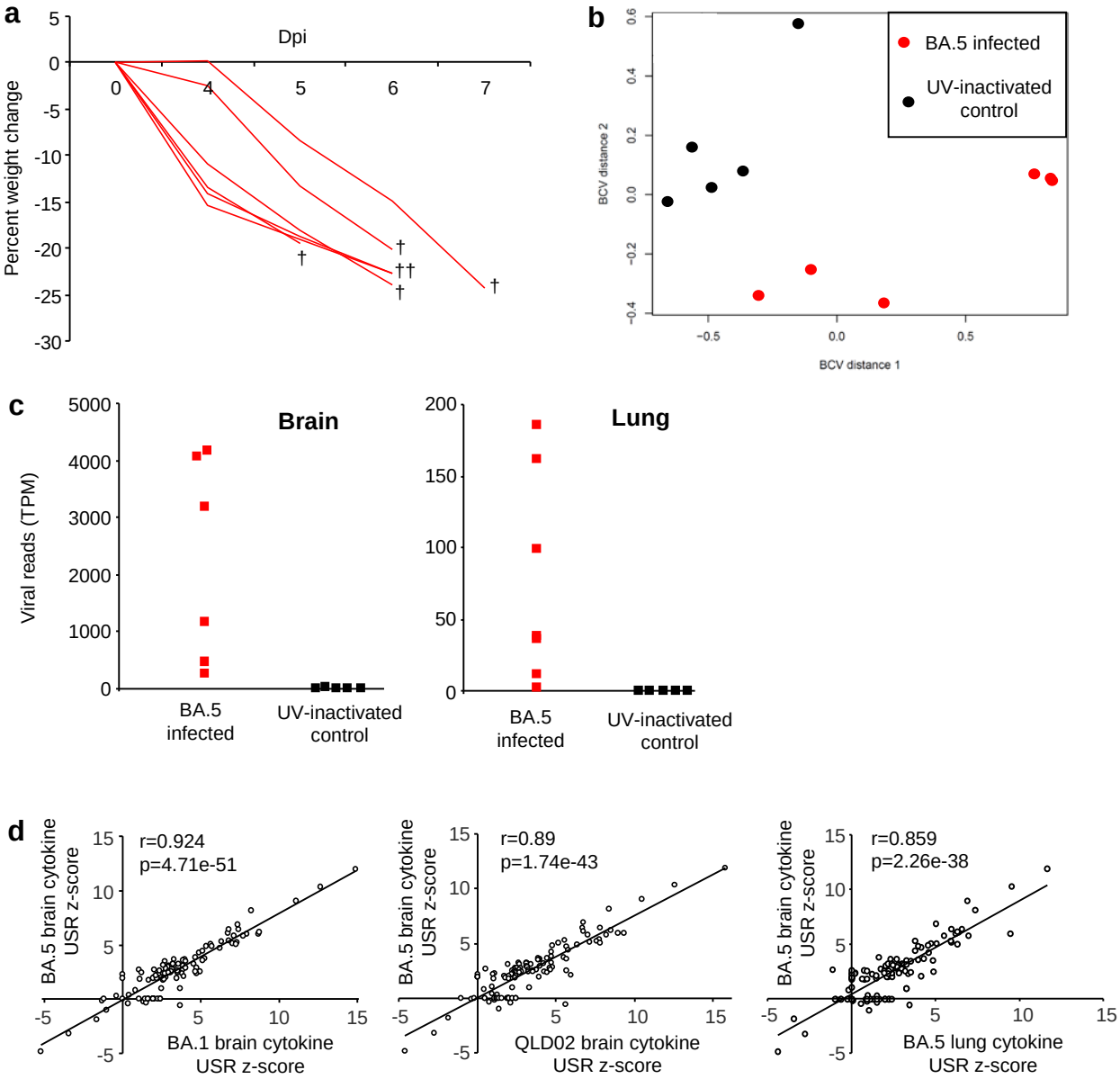

Supplementary Figure 5. RNA-Seq of brains from BA.5 infected K18-hACE2 mice.
a Weight loss for BA.5 infected K18-hACE2 mice used for RNA-Seq (no measurements were taken on 2 or 3 dpi). Half the brain was used for RNA-Seq and the other half was analysed by histology. Mice reached ethically defined end points on 5 dpi (n=1), 6 dpi (n=4), and 7 dpi (n=1), brains were harvested at these time points and used for RNA-Seq. **b** PCA plot showing segregation between brain samples from K18-hACE2 mice that were infected with BA.5 (n=6) or inoculated with UV-inactivated virus (n=5). **c** Viral and lung read counts (TPM). **d** Pearson correlations for cytokine IPA USR z-scores between indicated groups. When an USR was absent (not significant) for one group but present (significant) for the other, a z-score of 0 was given to the former. The BA.1 data set was derived from the 3 mice that died 9/10 dpi (n=3), with controls inoculated with UV-inactivated virus (n=5). The QLD02 data set was derived from the 5 mice euthanized 5 dpi (n=5), with brains from naive mice used as controls (n=5). The BA.5 lung data set was obtained from the same mice as for the brains.

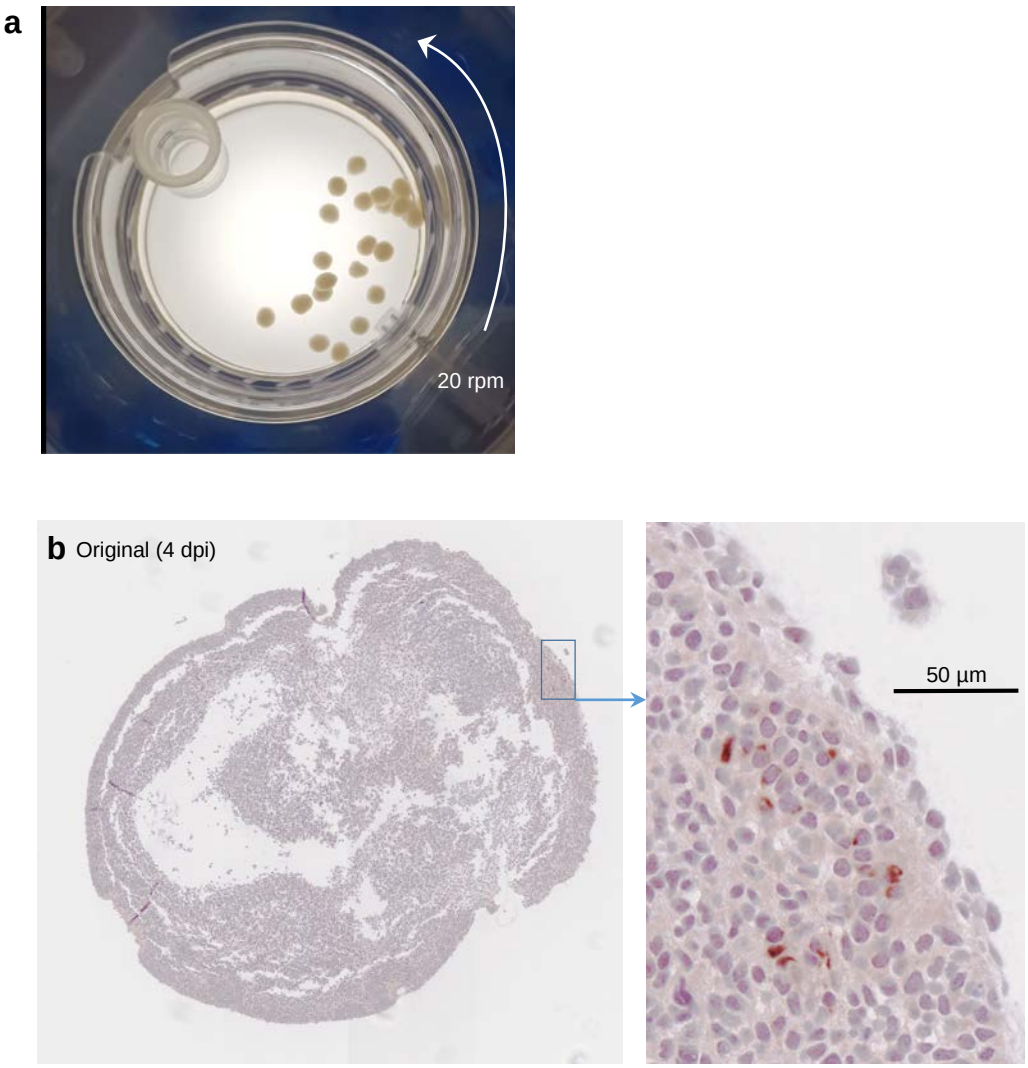

Supplementary Figure 6. Human cortical brain organoids. a Photograph of "mini-brains" grown in a rotating CelVivo Clinostar incubator. **b** hACE2 IHC for the organoid shown in Fig. 6c (original), corresponding to the region of viral infection.

a

SARS-CoV-2 (original strain) infected K18-hACE2 mouse brains and lungs

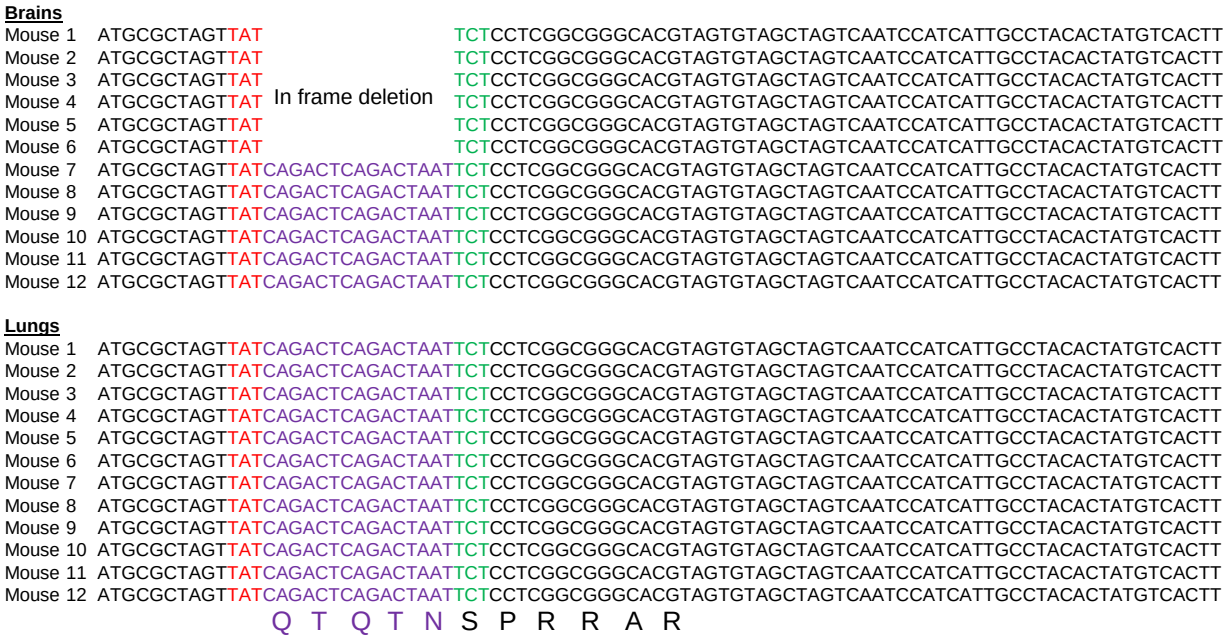

b

SARS-CoV-2 (original strain) infected hamsters brains and lungs (Frere *et al*. 2022. Sci Transl Med)

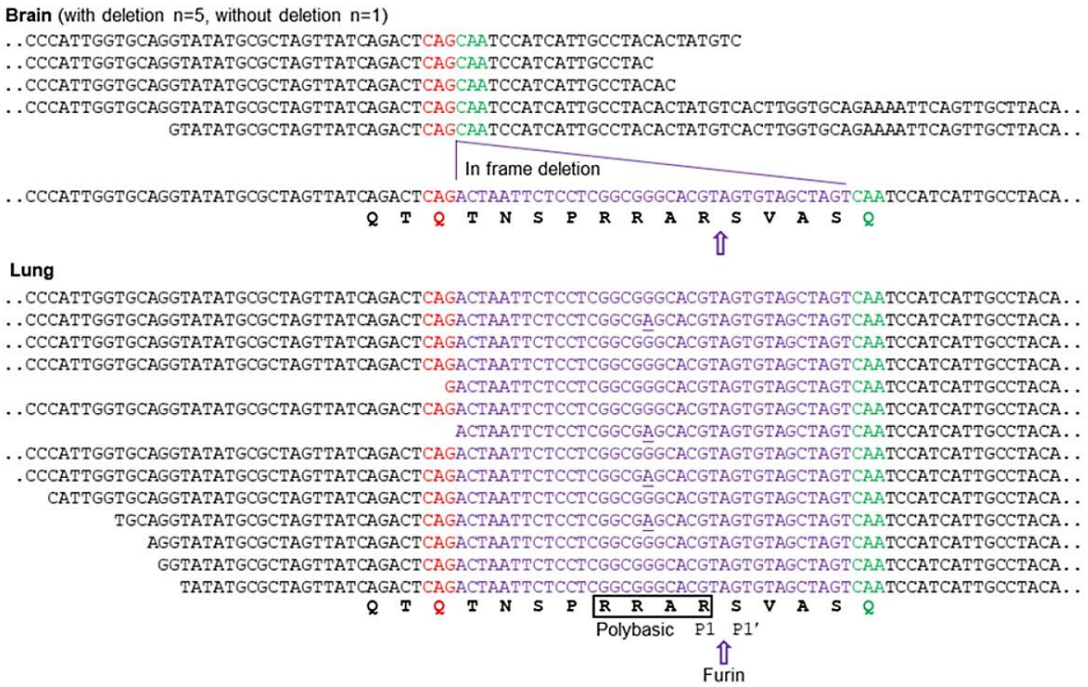

Supplementary Fig. 7. Virus in brains show loss of functional furin cleavage site. **a** K18-hACE2 mice infected with SARS-CoV-2 QLD02 strain (bioproject number: PRJNA813692). SARS-CoV-2 sequences in 6/12 mouse brains had a deletion of the QTQTN flanking sequence of the furin cleavage site, while this site was intact in lungs of the same mice. **b** RNA-seq data from brains and lungs of hamsters infected with SARS-CoV-2 original strain (WA1) was downloaded from SRA Bioproject PRJNA837993 (Frere *et al*. 2022. Sci Transl Med). RNA-Seq bioinformatics was performed as described in the methods and virus sequences viewed in Integrated Genomics Viewer. 5/6 sequence reads spanning this region in the brain had deletions in the furin cleavage site (TNSPRRARSVAS). This deletion was not identified in any lung sequences.